Pervasive aqueous paleoflow features in the Aeolis/Zephyria Plana region, Mars

Devon M. Burr [a,b,*], Marie-Therese Enga [c], Rebecca M.E. Williams [d], James R. Zimbelman [e], Alan D. Howard [f], Tracy A. Brennand [g]

[a] *Earth and Planetary Science Department, University of Tennessee Knoxville, 306 EPS Building, 1412 Circle Dr., Knoxville, TN 37996-1410, United States*
[b] *Carl Sagan Center for the Study of Life in the Universe, SETI Institute, 515 N Whisman Rd, Mountain View, CA 94043, USA*
[c] *Department of Physics and Astronomy, Northern Arizona University, Box 6010, Flagstaff, AZ 86011-6010, USA*
[d] *Planetary Science Institute, 1700 E. Fort Lowell, Suite 106, Tucson, AZ 85719-2395, USA*
[e] *Center for Earth and Planetary Sciences, MRC 315, National Air and Space Museum, Smithsonian Institute, Washington, DC 20013-7012, USA*
[f] *Department of Environmental Sciences, University of Virginia, P.O. Box 400123, Charlottesville, VA 22904-4123, USA*
[g] *Department of Geography, Simon Fraser University, 8888 University Drive, Burnaby, BC, V5A 1S6 Canada*

ARTICLE INFO

ABSTRACT

A survey of THEMIS visible wavelength images in the Aeolis/Zephyria Plana region over the two western lobes of the equatorial Medusae Fossae Formation (MFF) shows ∼150 sinuous ridges having a variety of morphologies and contexts. To systematize investigation, we use a classification scheme including both individual ridge and ridge network types, as well as associations with impact craters and fan-shaped features. The morphology of the ridges, their location downslope from higher topography (e.g., crater rims and scarps), and their association with fan-shaped forms indicate that most sinuous ridges formed through overland aqueous flow. Analysis of observations by individual ridge type leads to interpretation of most of these sinuous ridges as inverted fluvial channels or floodplains and a few as possible eskers, with the origin of the remaining ridges under continuing investigation. About 15% of the sinuous ridges are associated with impact craters, but data analysis does not support a genetic relationship between the craters and the sinuous ridges. Instead, analysis of one sinuous ridge network associated with a crater indicates that the water source for the network was atmospheric in origin, namely, precipitation runoff. The broad areal distribution of these ∼150 ridges and the network morphologies, in particular the branched and subparallel types, suggest that an atmospheric water source is generally applicable to the population of sinuous ridges as a whole. This concentration of sinuous ridges is the largest single population of such landforms on Mars and among the youngest. These ridges are situated at a paleoscarp between Cerberus Palus and the Aeolis highlands, suggesting that the precipitation that formed them was orographic in origin. The ages of the equatorial MFF units in which this population of sinuous ridges is found imply that this orographic rain and/or snow fell during some period from the late Hesperian through the middle Amazonian.

© 2008 Elsevier Inc. All rights reserved.

1. Introduction

Zephyria Planum, located at 0° N 165° E, is centered near the middle of the Cerberus plains (Fig. 1). The Cerberus plains are one of Mars' youngest regions, filled with very late Amazonian lava (Hartmann and Berman, 2000). Aeolis Planum, also near Mars' equator, is centered at 3° S, 140° E along Mars' highland-lowland boundary. This boundary is a global transition zone that divides the heavily cratered southern highlands from the lightly cratered northern lowlands. The dichotomy boundary in the Aeolis region is characterized by steep scarps and fretted terrain, which are hy-

pothesized to be a product of combined fracturing and aeolian erosion (Irwin et al., 2004). The cause(s) and timing of this dichotomy boundary remain ambiguous, with hypotheses including both endogenic and exogenic mechanisms (see Irwin et al., 2004 for a summary).

Between the Aeolis and Zephyria Plana are located the two western-most lobes of the Medusae Fossae Formation (MFF), which extend from the dichotomy boundary northward into the Cerberus plains (Fig. 1). The MFF is an extensive equatorial unit located along the global dichotomy boundary between 130° and 240° E (Bradley et al., 2002). Crater counts and observed superposition relationships among geologic units lead to an age determination for the MFF as Amazonian (Tanaka, 1986; Werner, 2006), although earlier work suggests it could be older (Schultz and Lutz-Garihan, 1981). The MFF exhibits nearly ubiquitous 10- to 100-meter scale linear or lemniscate hills interpreted as yardangs,
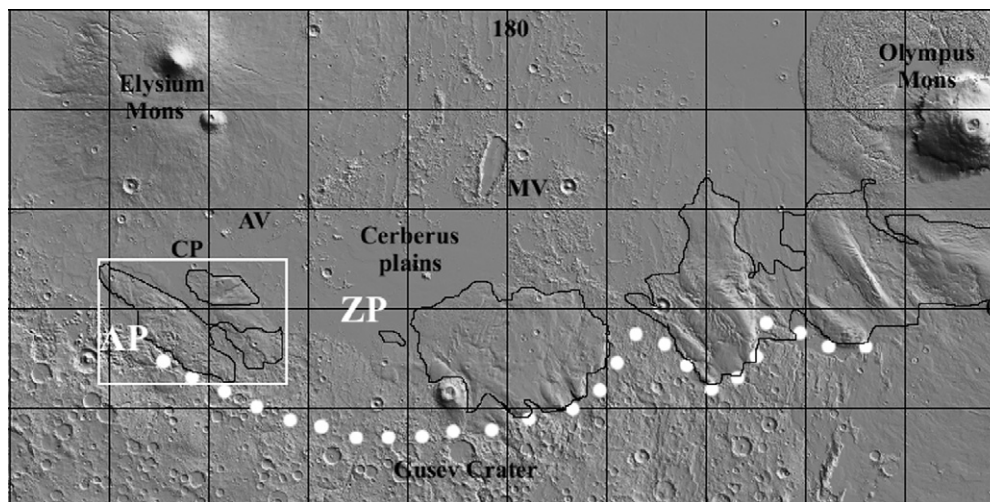
Fig. 1. Shaded relief MOLA topography of the Aeolis/Zephyria Plana region of Mars showing regional context. Major features are labeled; AV denotes Athabasca Valles, MV denotes Marte Vallis. The white dots show the dichotomy as mapped by Scott and Tanaka (1986) and Greeley and Guest (1987) with a generalized, simplified outline of the Medusae Fossae Formation (MFF) in black north of it. The white box outlines the study region (Fig. 9)—the two western lobes of the MFF. 'AP' denotes the center of Aeolis Planum, 'ZP' denotes the center of Zephyria Planum, and 'CP' denotes the center of Cerberus Palus. The black grid is in units of 10 degrees, and shaded relief illumination is from the upper right.

which result from aeolian erosion (Ward, 1979; El-Baz et al., 1979; Scott and Tanaka, 1982; Wells and Zimbelman, 1997). The origin of the MFF is uncertain; a volcanic air fall deposit is considered most consistent with recent data, but aeolian deposits, pyroclastic flow, or mixed volcanic sedimentary flow and fall deposits are also possible (see Bradley et al., 2002; Hynek et al., 2003; Mandt et al., 2008). Thus, the Aeolis/Zephyria region is hypothesized to be the locus of a variety of geologic processes, showing aeolian, volcanic, and tectonic geomorphologies.

In this paper, we present features that we hypothesize to be indicative of channelized aqueous paleoflow in the Aeolis/Zephyria plana region. These features are sinuous ridges (examples shown in Figs. 2–8) concentrated on the two western-most lobes of the MFF. Limited examples of these features have been shown previously (Nussbaumer et al., 2003, Nussbaumer, 2005, 2007; Irwin et al., 2005; Williams and Edgett, 2005; McMenamin and McGill, 2005; Burr et al., 2006). For this work, we surveyed all Thermal Emission Imaging Spectrometer (THEMIS) visible wavelength images through the July 2007 release (resolution 18–36 m/px), along with selected images from the Context Camera (CTX) (resolution 6 m/pix), the Mars Orbiter Camera (MOC) (resolution 0.5–20 m/px), and the High-Resolution Imaging Science Experiment (HiRISE) (resolution 0.25–0.35 m/px). We also examined the global THEMIS day infrared (IR) mosaic and MOC wide-angle mosaics available at http://jmars.asu.edu/data/ to fill in data gaps in THEMIS visible image coverage. These additional data show that some of the sinuous ridges that appear disconnected THEMIS visible coverage are or may have been connected. However, for this initial work, we have not yet investigated those connections systematically: here, we parse the ridges based on THEMIS visible coverage. The THEMIS visible images and image mosaics used in this work are available from the authors in the form of Integrated Software for Imagers and Spectrometers (ISIS) (Gaddis et al., 1997) files.

From this survey, we classify the ridges morphologically and note associations with other geologic features (Table 1). On the basis of morphology and geologic associations, we assess formation mechanisms, the most likely of which include flowing water. We also give the ridges' geographic position (Fig. 9) and time-stratigraphic unit based on previously published work (cf. Greeley and Guest, 1987) (Table 1). In general, age-dating of Martian surfaces based on crater statistics is subject to question based on the evidence for both wide-spread mantling and exhumation (e.g.,

Greeley et al., 2001), as well as evidence of efficient secondary production (McEwen et al., 2005). In particular, discrimination of units in the MFF using crater densities as a proxy for deposition age is difficult because of aeolian erosion. On-going mapping of this region by one of us (JRZ) may significantly improve MFF unit boundaries and/or ages from those previously published. However, these published unit boundaries provide a first estimate as to the ridges' age.

We then discuss the regional and global context of these ridges, including their absence from the eastern MFF. Finally, we outline their implications, including orographic precipitation at the equator during the Amazonian. A total of 152 sinuous ridges are listed in Table 1. However, this number is subject to revision with further investigation, as increased data coverage may discover more sinuous ridges and/or show some of these enumerated sinuous ridges to be connected.

2. Sinuous ridges (SR): Morphologic classification and geologic associations

We use the term sinuous ridge (SR) to denote any elongate, positive-relief landform that is distinct from the usually shorter, straighter, mutually adjacent hills, inferred to be yardangs, that are visible throughout the MFF (e.g., Fig. 2). We have referred to similar landforms elsewhere on Mars as raised curvilinear features (RCFs) (e.g., Burr et al., 2006; Williams et al., 2007); sinuous ridges (SRs) are simpler. The SRs show a wide variety of cross-sectional and planform shapes, network patterns, and landform associations. To provide structure for this work, we have organized these features with a qualitative classification scheme that includes both individual and network classification. In most cases, these characteristics form a continuum among the classification types. Also, an individual feature or network of features may exhibit more than a single classification type. In both these cases, classification was assigned based on the perceived dominant appearance in the available data. Continued investigations with additional data may adjust these initial classifications.

2.1. A. Individual SR morphologies

Classification of individual SRs is based largely on SR width and apparent cross-section shape, along with additional morphological characteristics that show an association with each type. For brevity,
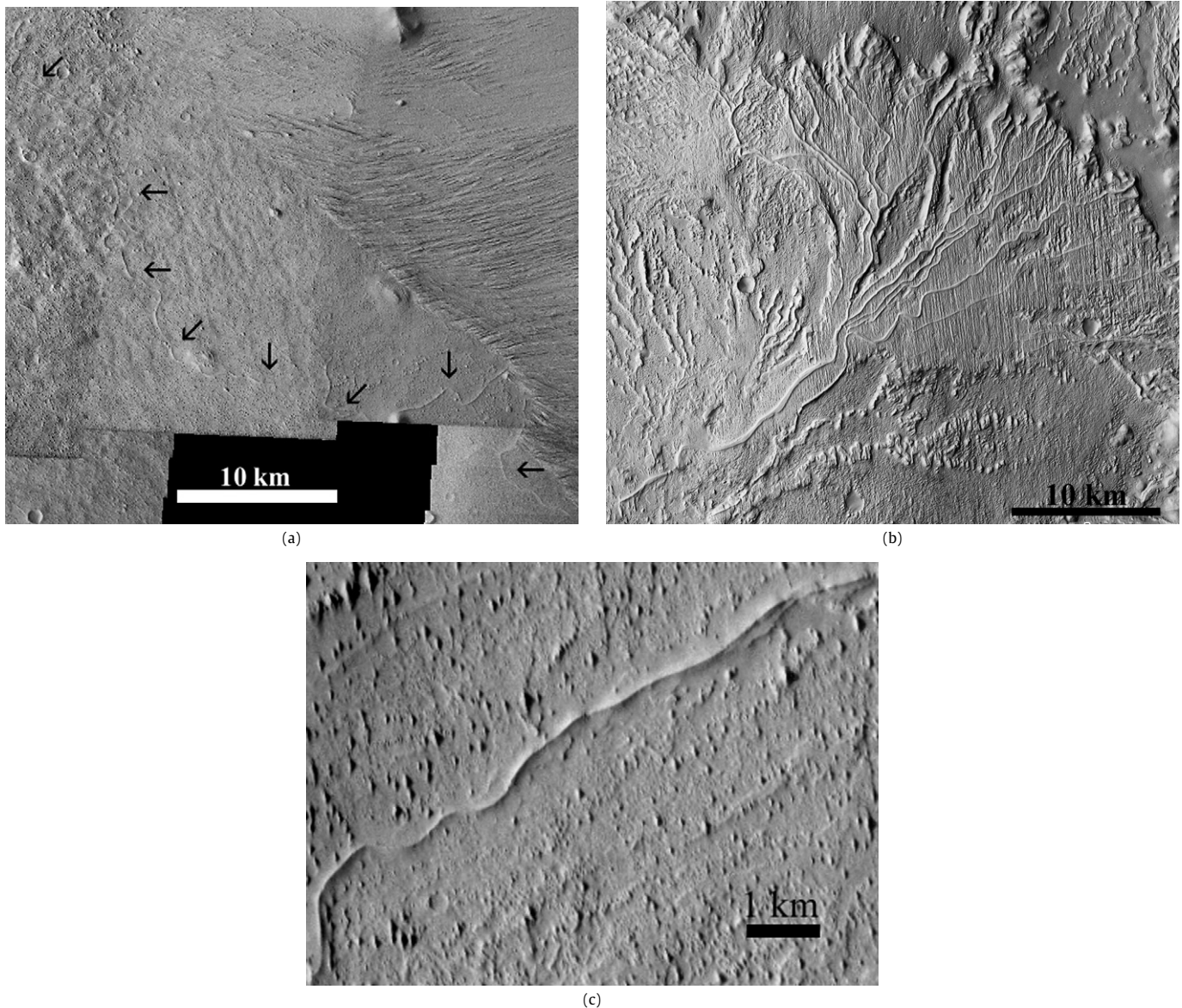
(a)

(b)

(c)

Fig. 2. Examples of thin SRs. On all images, north is up and illumination is from the left. (a) THEMIS image mosaic showing an isolated, thin SR (Area01, Table 1; located near 2.9° S 152.0° E) denoted by the arrows. The sub-parallel lineations at image right are inferred yardangs. (b) CTX mosaic showing a branched network of thin SRs (Area43_C, Table 1; located near 6.2° S 151.6° E). Extensive yardangs are oriented NNW-SSE across image. (c) Portion of THEMIS image V18393002, showing an isolated, thin SR (Area31_C, Table 1; located near 4.8° S 151.3° E) with a sharp medial ridge. The short, lemniscate hills oriented NW to SE throughout the image are inferred yardangs.

each type is denoted with a single adjectival term. A qualitative synopsis of the frequency and location of each individual SR type is provided in Fig. 9, and the relative frequency of individual types is summarized in Table 2.

2.1.1. Thin

Thin SRs (Fig. 2) are a few tens of meters in width, and their width remains fairly constant along their length, although where several thin SRs connect with a single SR, the width of the single SR tends to be greater than the widths of the several individual SRs (Fig. 2b). Several have sharp medial crests that distinguish them from flat or rounded SRs (e.g., Fig. 2c). Thin SRs are the most common individual ridge type, comprising 34% of all SRs (Table 2). Thin SRs are also the most broadly distributed (T, Fig. 9), and located at a range of elevations from −960 to −2500 m. They have the widest variety of context, being found adjacent to impact craters, at scarps, and on flat terrain. The majority of thin SRs are on low terrain between or adjacent to the higher-standing MFF lobes.

2.1.2. Rounded

Rounded SRs are intermediate in width between thin and flat SRs, with transverse dimensions of several hundred meters and a relatively constant width along their length. Rounded SRs give the appearance of having a smooth shape in cross-section without sharp medial ridges or lateral edges (Figs. 3 and 8a). Geographically, rounded SRs define a swath oriented northwest-southeast within the broad topographic depression between the two western MFF lobes (R, Fig. 9). They are found on topographically flat terrain that has eroded into yardangs, and are not associated with scarps or impact craters. The rounded SRs are all Isolated (see 'Network Patterns' below; Table 2) and are located within a narrow elevation range between −2460 and −2550 m. They tend to be the longest SRs observed, commonly greater than several kilometers in length. The single exception to these rules is a short rounded SR that ends in a fan-shaped form (see Section 2.4 below and Fig. 8a). Rounded SRs are the rarest individual SR type, comprising only ∼5% of the total number of SRs (Table 2).
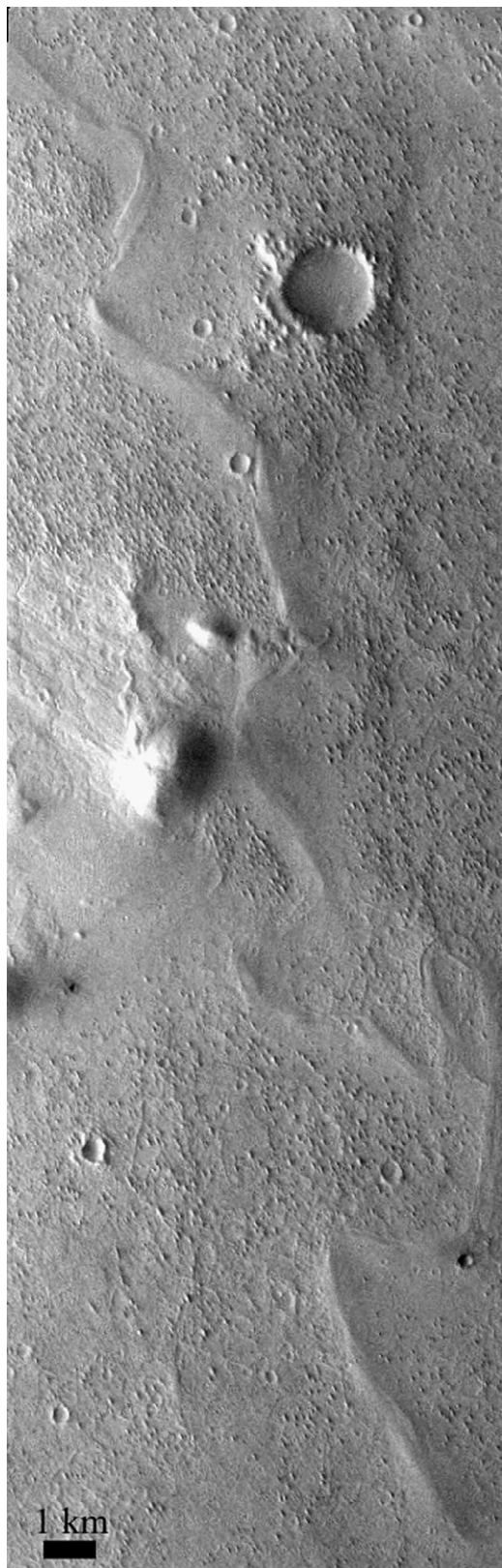
Fig. 3. Portion of THEMIS image V15011001, showing an isolated, rounded SR (Area38_C, Table 1; located near 3.8° S 151.8° E). North is up and illumination is from the left.

2.1.3. Wispy

Wispy SRs (Fig. 4) are the narrowest SRs, with widths of order ten meters. They are also short in length compared to other SRs. With these dimensions, wispy SRs are near the edge of detection in THEMIS visible images, and because of their small size, are usually identifiable only in groups. They commonly have low sinuosity compared with SRs of other classes. Wispy SRs comprise 13% of all SRs (Table 2) and have a wide geographic distribution (W, Fig. 9).

2.1.4. Flat

Often greater than a kilometer in width, flat SRs have broad and flat upper surfaces, which may stand above surrounding terrain with sharp lateral edges and steeply dipping sides (Figs. 5a, 5b, 5d, 6, 7a). In higher resolution imagery, these flat upper surfaces often exhibit numerous narrow, semi-concentric or sub-parallel, curved ridges (Fig. 5b). Flat SRs are the second most common individual ridge type, accounting for 30% of all SRs (Table 2). In comparison to thin and rounded SRs, flat SRs may show noticeable variation in width with distance along their length. They are almost entirely located around the circumference of the topographic depression between the two western MFF lobes or along the scarp adjacent to the Aeolis Planum highlands (F, Fig. 9), within an elevation range of −2750 m to −2100 m. A few additional examples occur at higher elevations adjacent to or on the topographic step that defines the highland-lowland boundary between Aeolis Mensae and the western MFF lobes (Fig. 1), and forms the contact between Amazonian and Noachian units (Greeley and Guest, 1987). In these locations, flat SRs commonly extend from these scarps into adjacent, topographically lower terrain. A single flat SR occurs at −2680 m on Cerberus Palus (Fig. 5d).

2.1.5. Multilevel

Multilevel SRs (Figs. 5a, 5c, 5e, 7a, 8b) denote any stacked combination of SR types. In multilevel SRs, the bottom or subjacent SR is always flat and the upper or superjacent SR is thin (Figs. 5a, 5e, 7a, 8b) or, rarely, wispy. In higher resolution images, the lower, flat surfaces of multilevel SRs may exhibit narrow, semi-concentric or sub-parallel, curved ridges (Fig. 5c). To be categorized as multilevel, the network pattern of each SR level must align (i.e., SRs that intersected underlying flat SRs at an angle and/or did not lie entirely on the lower SR were categorized separately and not as multilevel). Like flat SRs, multilevel SRs commonly extend from scarps onto lower elevation terrain. They make up 18% of the total SRs in this study (Table 2) and have a wide geographic distribution (M, Fig. 9).

2.2. Network patterns

Classification of SR networks is based on typical junction angles between the individual SRs in the network, along with any subsidiary characteristics as noted in the text. Comprehensive quantitative data are not available, but approximate ranges of junction angle values are provided. From this initial analysis, no clear association is apparent regarding geographic distribution by network type. The frequency of each SR network type is provided in Table 2.

2.2.1. Isolated

An isolated SR refers to a single SR that is not connected or closely adjacent to other SRs within the field of view of THEMIS visible wavelength images available to date (Figs. 2a, 2c, 3, 5d, 5e, 8a). Isolated networks account for 22% of all SRs identified here (Table 2). All rounded SRs are isolated.

2.2.2. Sub-parallel

In a sub-parallel network, the individual SRs are aligned roughly parallel to one another or intersect with low (<∼30°) junction angles (Figs. 5a and 7a). They are often connected at one end to a common area. If they join, they do so with less frequency and at smaller angles than do branched or random SRs. Sub-parallel networks account for 27% of all SRs in this study (Table 2).
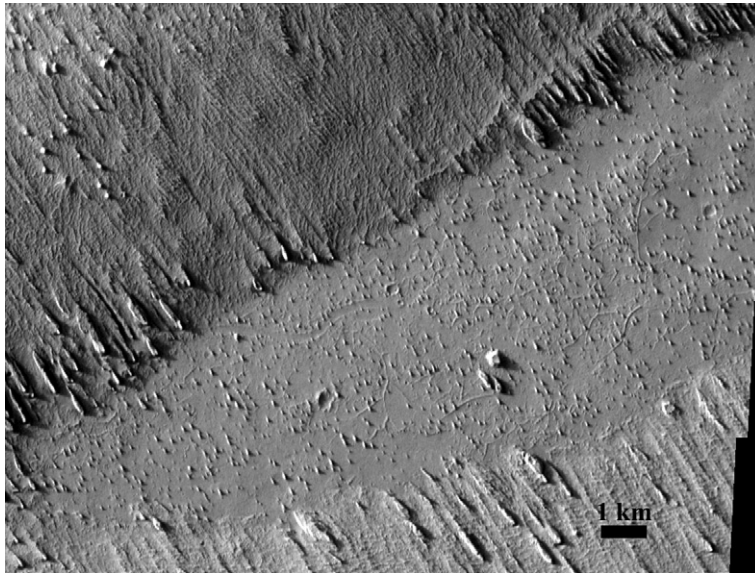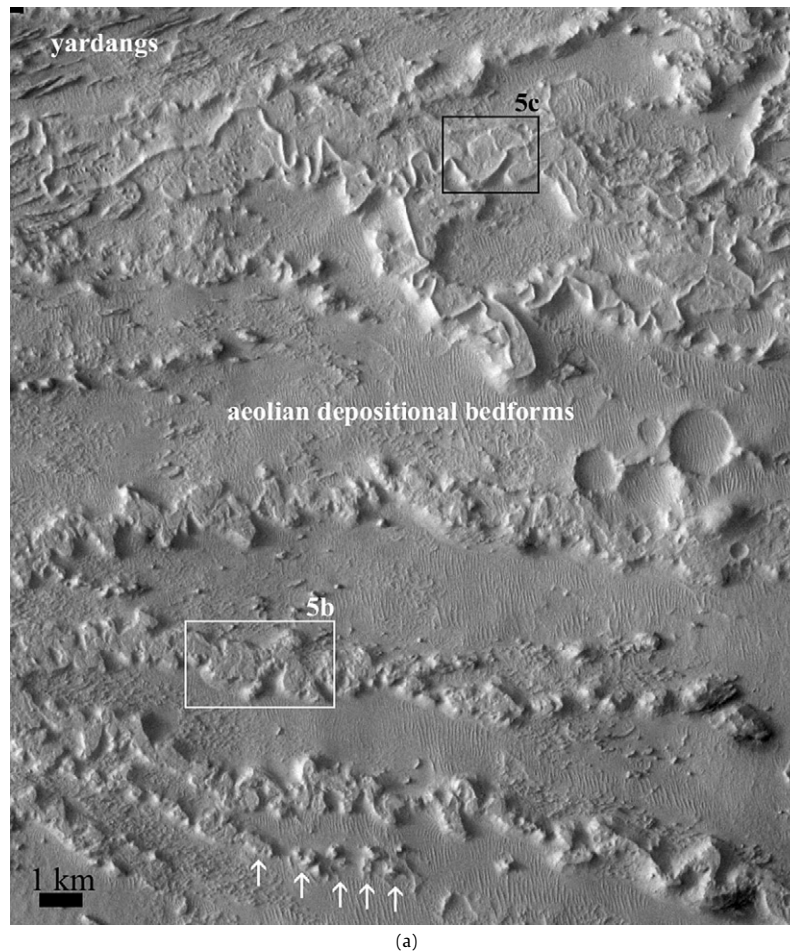
Fig. 4. Portion of THEMIS image V13163010, showing a random network of wispy SRs (Area04, Table 1; located near 2.1° N 153.8° E). The NW-SE-oriented lemniscate forms at upper left and lower right are inferred yardangs. A sinuous trough of unknown origin is visible near image center. North is up and illumination is from the left.

(a)

Fig. 5. Examples of flat and multilevel SRs. In all images, north is up and illumination is from the left. (a) Portion of THEMIS image V05875001, showing two SRs. The northern SR network is a branched network of multilevel (thin on flat) SRs (Area35_E, Table 1; located near 4.9° S 154.9° E). The southern network is a sub-parallel network of flat SRs (Area35_F, Table 1; located near 5.1° S 154.7° E). The white and black boxes show the locations of (b) and (c), respectively. The white arrows indicate where the flat SR has transitioned into disjoined knobs. The larger NE-SW lineations in the upper left corner are inferred yardangs; the fine NW-SE lineations among the SRs are inferred aeolian depositional bedforms. (b) Portion of CTX image P06_003215_1752_XI_04S205W, showing the surface texture of a flat SR. The white arrows point to sub-parallel curved lineations. (c) Portion of CTX image P06_003215_1752_XI_04S205W, showing the surface texture of a multilevel SR. The white arrows point to sub-parallel curved lineations on the lower, flat SR; the black arrows point to the superposed thin SR. (d) Portion of THEMIS image V05899007 showing an isolated, flat SR (Area26, Table 1; located near 4.8° N, 155.2° E) on Cerberus Palus (black arrows) that appears to transition into negative relief (white arrows). (e) Portion of MOC image R20-00313 showing a close-up view of an isolated, multilevel SR (thin on flat) (Area26, Table 1; located near 5.5° S 151.3° E) cross-cut by yardangs.

(b)

(c)

(d)

(e)
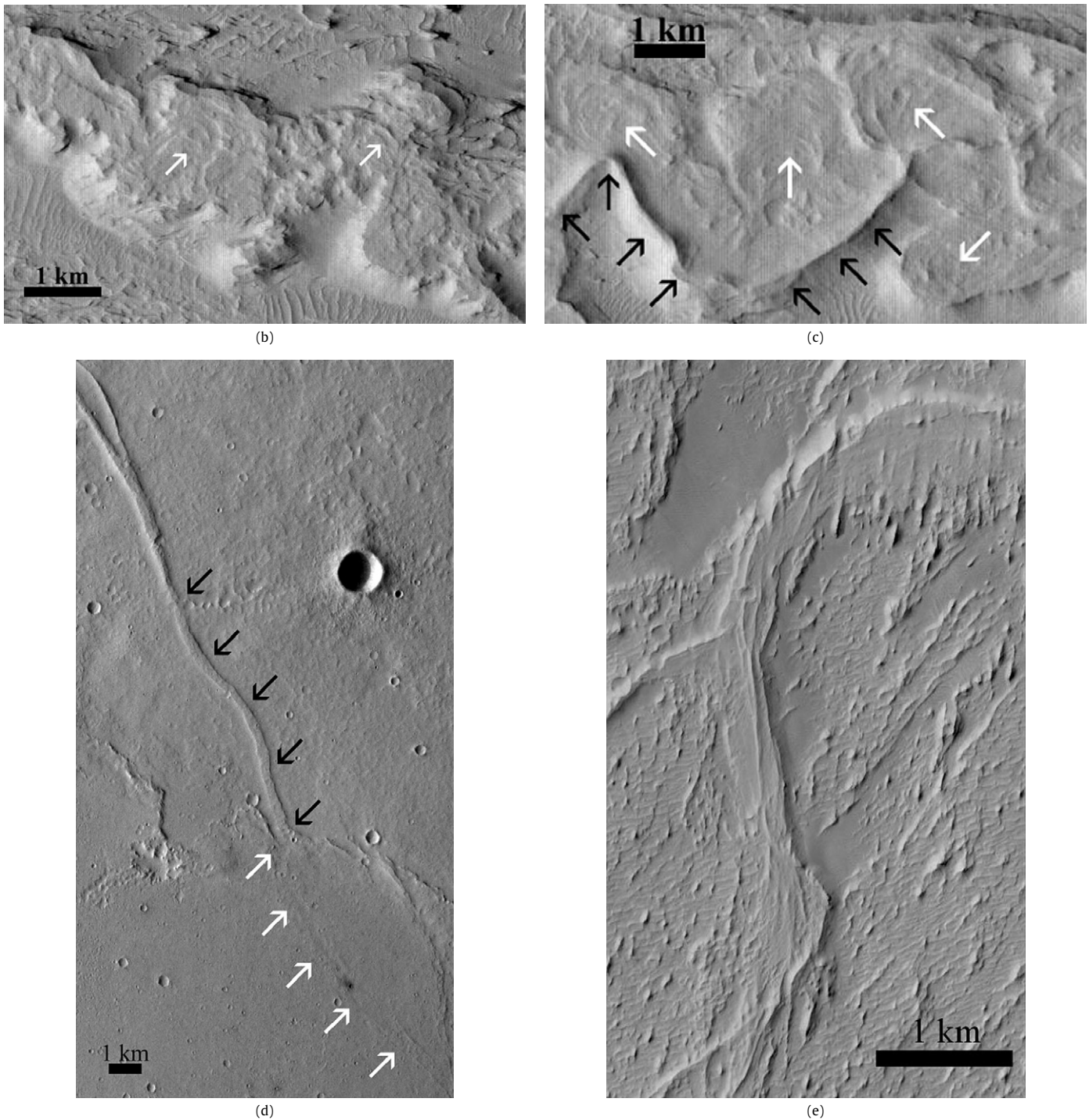
Fig. 5. (*continued*)

2.2.3. Branched

A branched network of SRs refers to individual SRs that intersect at moderate (∼30° to ∼75°) angles (Figs. 2b and 5a) forming a network typically on the order of tens of kilometers in width. Typically these are low order networks, but a representative sampling of network order has not been attempted. This category includes what are probably dendritic, tributary and/or distributary networks, although uncertainty regarding flow direction precludes use of those more specific terms. Branched networks are the most prevalent network type, comprising 41% of the total (Table 2).

2.2.4. Random

Random SR networks have ridges that intersect at large (>∼75°) angles, a wide range of intersection angles, and/or lack obvious directional trends (Fig. 4). Random SR networks are the least common network type, making up 10% of all mapped SRs (Table 2).

2.3. Association with impact craters

Approximately one-seventh of the total number of identified SRs is associated with impact craters. In order to be classified as having impact crater association, the SR must be contiguous with a
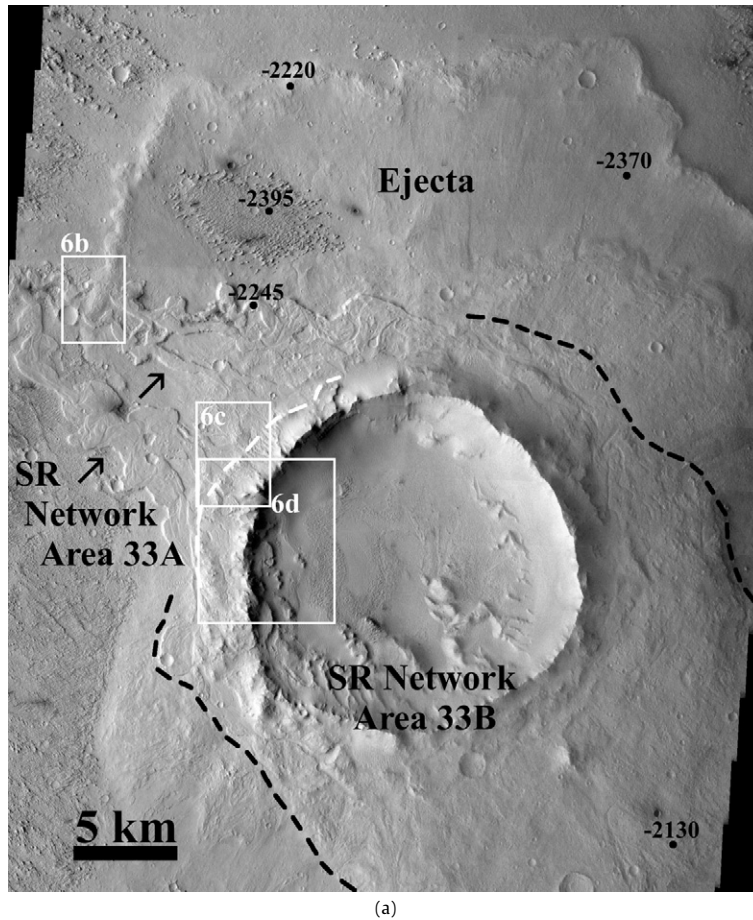
(a)

Fig. 6. (a) THEMIS visible image mosaic showing a branched, flat SR that is associated with an impact crater (black arrows point to Identifier Area33_A, Table 1; located near 5.7° S 154.7° E). The SR stretches around the north side of the crater, where it overlies the fluidized impact ejecta. The dashed black lines indicate the area that appears slightly elevated, and encompass possible SRs, poorly exposed, on either side of the crater. The white dashed line shows the location of the small scarp at the base of the crater rim. The black numbers give approximate elevations (the three points on the left are from MOLA track 12220, the two points on the right are from MOLA track 10672). The white boxes show the locations of (b), (c), and (d). North is up, and illumination is from the left. (b) Portion of CTX image P05_003149_1750, showing locations where the SRs occupy local minima in the ejecta rim. The southern black arrows point to a trough in which the SR lies. The northern arrow likewise points to a trough, although the SR appears to have been eroded at this point. (c) Portion of CTX image P05_003149_1750. The black horizontal arrows show examples of sinuous troughs cross-cutting SRs, and the white vertical arrows show examples of sinuous troughs connecting with SRs. The white dashed line shows the location of the small scarp at the base of the crater rim. (d) Portion of CTX image P05_003149_1750, showing sinuous troughs that extend both out from the crater and down into the crater. The continuation of a sinuous trough as a SR on the crater floor is outlined in white dots, and slump blocks that have translocated from the sharp-edged crater rim are labeled.

crater that is wider than the SR itself (Figs. 6a and 7a). The purpose of this condition is to focus on those impact craters that are large enough compared to their associated SRs that they might have a genetic relationship with those SRs. However, any such relationships remain to be demonstrated (see Section 3.3.3 below).

2.4. Association with fan-shaped forms

About 5% of the SRs are connected to forms that are fan-shaped in plan-view. In data available to date, fan-shaped forms can be seen at the ends of SRs of all individual ridge types except flat (Table 1). Most fan-shaped forms have arcuate margins; some margins are more digitate (Fig. 8a). Fan-shaped forms are of the order of a few kilometers in width and are characterized by having relatively straight ridges on their surfaces that connect to the end of the associated SR and are oriented radially with respect to that location. Of the seven fan associations recorded in Table 1, Area37 (Fig. 8a) and Area06_C (Fig. 8b) contain the best-formed fans. Other fan-shaped forms recorded in Table 1 are less distinct (e.g., Area18_ B) or their trunk SR has been eroded into a sinuous string of adjacent knobs (Area45_L and 45_M, cf. discussion in Section 3.3.1, below).

We differentiate these fan-shaped forms from more extensive branched networks of SRs in which the individual SRs are radi-

ally oriented (e.g., Fig. 2b). Both fan-shaped forms and branching networks can have radial ridges and comprise a continuum of landforms, but are distinct from each other in terms of size, ridge sinuosity, and the overall apparent topographic form. Branched networks are significantly larger in size (of order tens of kilometers in width) in comparison to fan-shaped forms (of order kilometers in width). Also, the individual SRs in these branched networks are more sinuous than the radial ridges on the fan-shaped forms. In addition, the flow directions in the branched networks (e.g., Fig. 2b) are somewhat ambiguous and so cannot indicate distributary over tributary paleoflow without future investigation. In contrast, all the classified fan-shaped forms appear to be located at the distal (lower) ends of the associated SRs and to decrease in elevation with distance from the SRs (Fig. 8). This elevational wedge shape supports an unambiguous inference of distributary paleoflow.

Some branched networks have kilometer-scale sizes and relatively straight, radial ridges as do other fan-shaped forms, but they lack some other important criterion for classification as fan-shaped forms. For example, they may grade into the surrounding terrain and so lack wedge-shapes, and/or they may lack associated trunk SRs. Examples include Area35_B and 35_D and Area45_N and 45_O. Their surface texture is similar to that of distinct fan-shaped

(b)

(c)

sinuous trough

slump
blocks
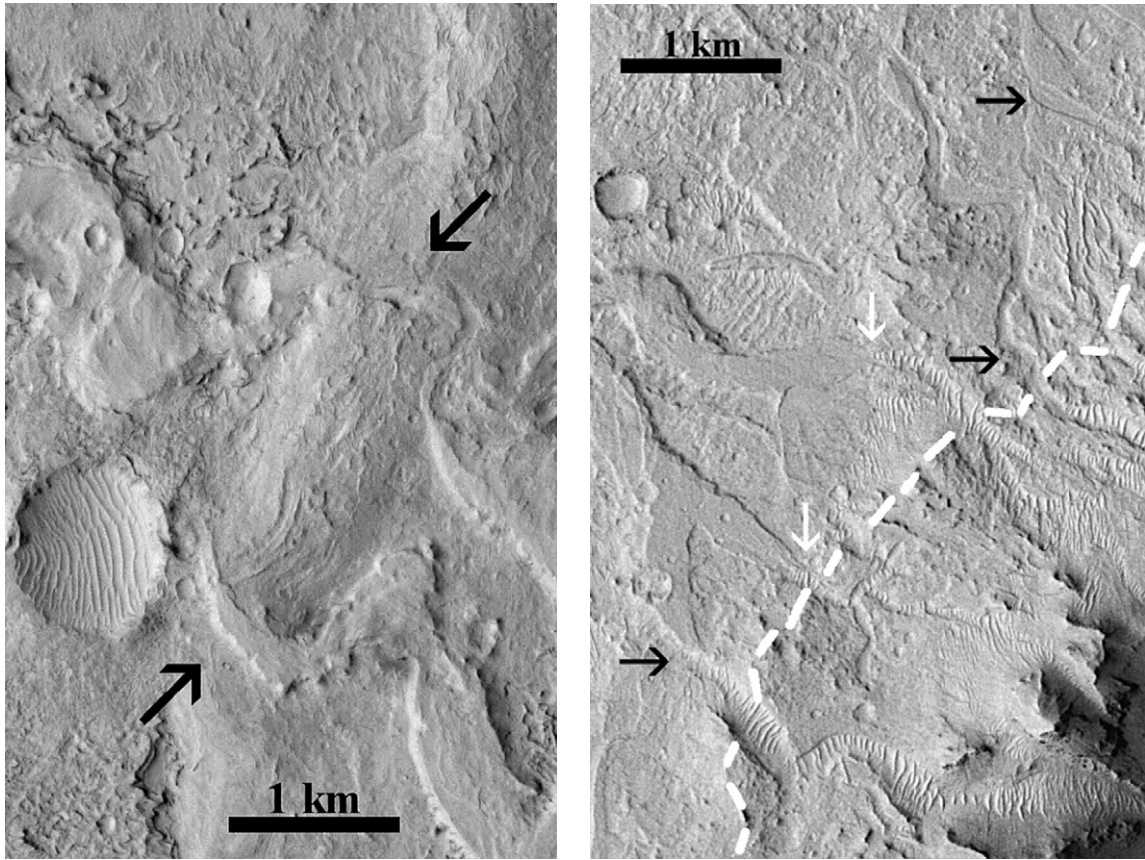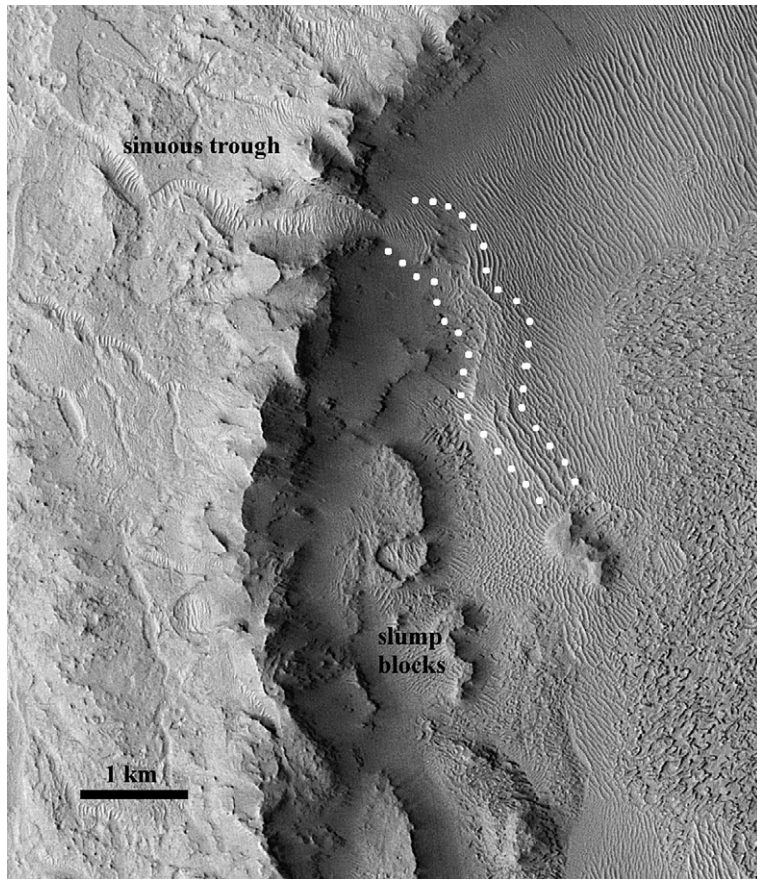
(d)

Fig. 6. (*continued*)

Fig. 7. SRs associated with impact craters. (a) THEMIS visible image mosaic showing two SRs associated with impact craters centered near 5.3° S 155.3° E. They are classified as sub-parallel based on THEMIS visible mosaics, although the global THEMIS day IR mosaic (b) shows that they connect to t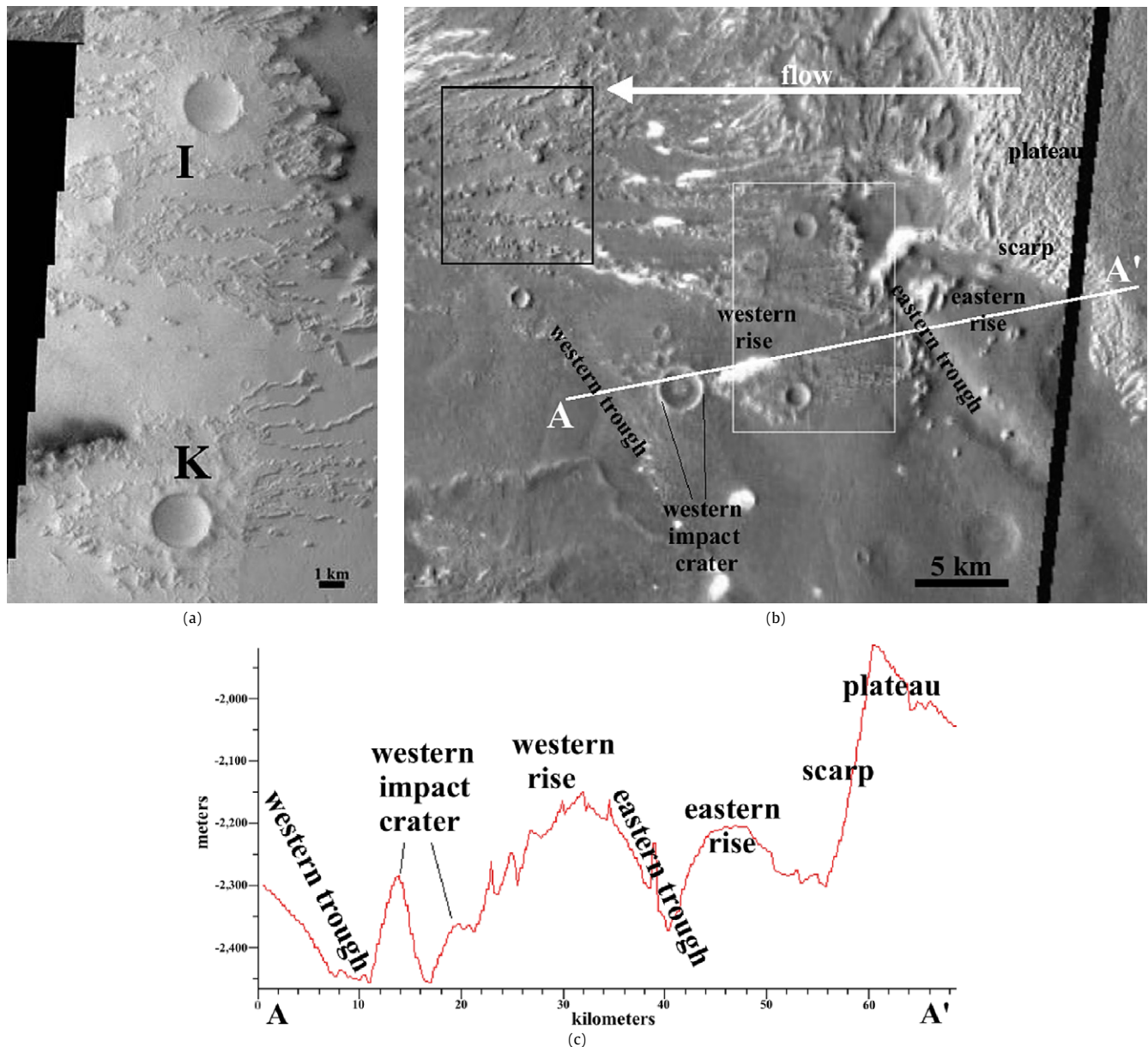he west. 'I' denotes a multilevel subparallel SR at Area35_I (Table 1). 'K' denotes a flat subparallel SR at Area35_K (Table 1). (b) A portion of the global THEMIS day IR mosaic showing regional coverage. The black box shows the location of Fig. 5a, the white box shows the location of (a), the white line (A–A′) shows the location of the profile in (c), and features discussed in the text are labeled. The big white arrow shows inferred flow direction. (Image credit for THEMIS day IR mosaic: NASA/JPL/Arizona State University.) (c) Profile (A–A′) of MOLA gridded topography across the area where the SRs in (a) and (b) are located. (Image credit for MOLA gridded topography profile: NASA/JPL/Arizona State University.)

forms, but because they lack associated trunk SRs and/or wedge-shapes, these examples cannot strictly be classified as fan-shaped forms. They are classified as branched SR networks and noted in Table 1 with asterisks in the 'FAN' category. Only in the cases where fan-shaped forms are distinct wedges that can be inferred to have been connected to trunk SRs are firm fan associations recorded.

3. Hypothesized origins of SRs

3.1. Non-aqueous origins largely discounted

Aeolian, structural/tectonic, and volcanic processes have been inferred to have operated in the Aeolis Planum region, but we do not find evidence to support these as the primary processes in SR formation. Aeolian processes may produce unusual yardangs

(Mandt et al., 2008), but we discount an aeolian processes as the primary origin for the SRs discussed here based on the greater SR length (up to several kilometers), more curvilinear plan-view morphology (planform), and/or orthogonal orientation relative to inferred yardangs (Ward, 1979; El-Baz et al., 1979; Scott and Tanaka, 1982; Wells and Zimbelman, 1997); SRs cross-cut yardangs or are cross-cut by them (e.g., Fig. 2b). We also discount a primarily structural/tectonic origin because although fracturing and associated processes (Irwin et al., 2004) may produce fretted terrain, the sinuosity of SRs is qualitatively greater than that of the fretted terrain.

The network appearance and sinuosity of the SRs suggest their formation by a channelized flowing fluid. This fluid could be either lava or water. Through levee buildup, lava channels can become positive-relief features. However, such lava channels would
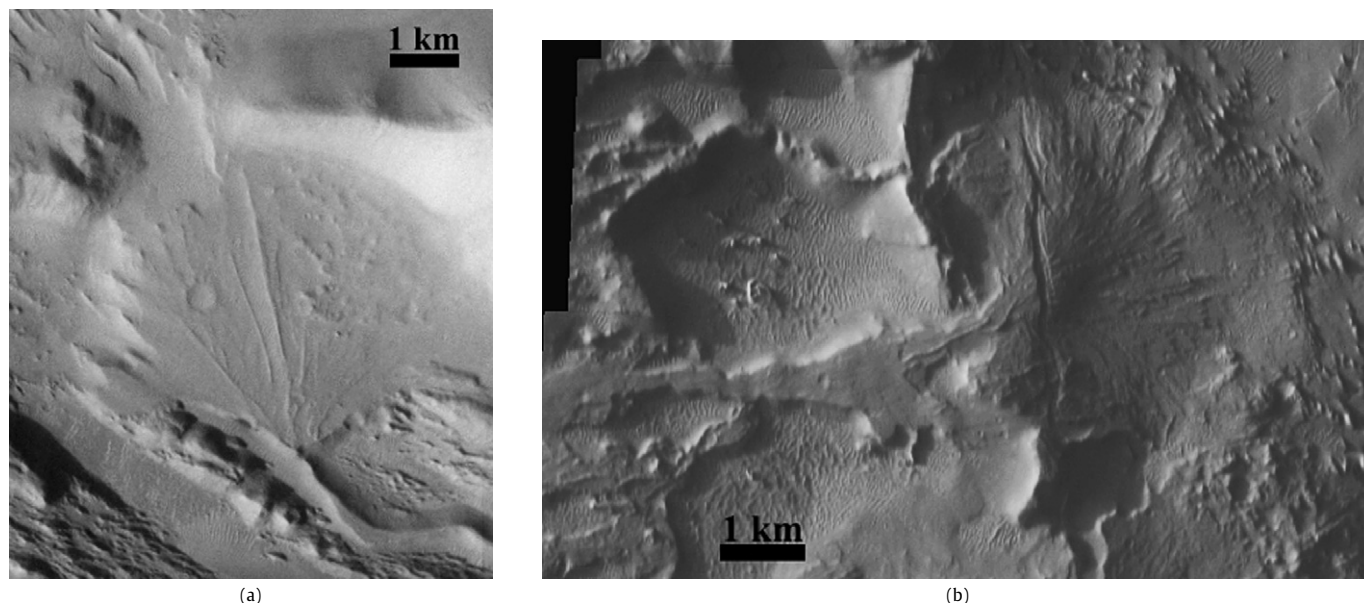
(a)   (b)

Fig. 8. Examples of SRs connected to fan-shaped forms. In both images North is up and illumination is from the left. (a) A rounded SR (lower right of image) connected to a fan-shaped form (image center) with radial ridges (from THEMIS image V16983002, Identifier Area37, Table 1; located near 6.2° S 145.5° E). (b) A branched multilevel SR (left of image) connected to a fan-shaped form (right of center) with radial ridges (from THEMIS image V13288011, Identifier Area6_C, Table 1; located near 0.2° S 146.4° E). The fan-shaped form sits within a crater, whose rim stretches north-south across the center of the image.

likely have two narrow, marginal ridges corresponding to the lava levees (see, e.g., Poland et al., 2008, Fig. 1). Topographic inversion of a lava channel to produce a single broad, flat-topped ridge could occur through denudation of surrounding material; for example, a lava channel formed in pyroclastic material would likely be more resistant to erosion than the surrounding material. The western MFF may be comprised of explosive volcanic sedimentary deposits (Bradley et al., 2002; Hynek et al., 2003; Mandt et al., 2008) that may have originally been more extensive, and Cerberus Palus is inferred to be composed of lava (Keszthelyi et al., 2000, 2004) (although see Murray et al., 2005, for an alternative explanation). Thus, based on its context and low sinuosity, the best explanation for the flat SR located on the Cerberus plains (Fig. 5d) might be as an inverted lava channel.

In comparison to the SR on the Cerberus plains, the large majority of these SRs have a higher sinuosity (e.g., Figs. 2a, 2b, 3, 5a, 6a, 7a, 7b), which is not characteristic of lava channels. In addition, the morphology of the thin SRs that display sharp central ridges (e.g., Fig. 2c) is inconsistent with formation by flowing lava. To produce lava channels at the observed elevations would require an elevated lava source, which is not (or no longer) apparent. Thus, although volcanism may have played some secondary role in SR formation such as through fluvial channel infill as part of the inversion process (e.g. Pain and Ollier, 1995; Rhodes, 1980; see Section 3.2.1 below), and although lava flow might be the origin of the flat SR on Cerberus Palus (Fig. 5d), we discount volcanism as the primary, or the most common origin, for the large majority of these SRs.

3.2. Formation by flowing water: possible terrestrial analogs

On the basis of SR linearity and sinuosity, the termination of a small number of SRs in fan-shaped forms, and the locations of many SRs down slope from relative elevation highs (impact crater rims or topographic scarps), we hypothesize formation of most SRs by flowing water. Flowing water can produce positive relief sinuous features in two ways: as topographically-inverted fluvial channels and as eskers.

3.2.1. Inverted fluvial channels

River channels form in (normal) negative relief and may then become inverted by denudation to form ridges (Fig. 10). This process occurs when the channel floor becomes more resistant to erosion than the surrounding terrain. This increased resistance could be a result of infill of the channel by lava, deposition by the river of a coarse-grained lag, or geochemical cementation of sediments. After the channel floor develops this increased resistance, regional erosional processes remove the surrounding terrain. In terrestrial examples, the eroded materials are commonly fine-grained fluvial overbank deposits (although in the present

Table 1

Listing of SR identifiers, locations, approximate elevation, and stratigraphic units (see footnote for explanation of abbreviations). Network types are given under 'NETWORK.' Geologic associations are given as 'CR' indicating a SR with a crater association, and 'FAN' indicating a SR with a fan-shaped form association. (SR fan-shaped forms that do not fully match the criteria given in Section 2.4 are marked under 'FAN' with an asterisk.) Individual SR types are indicated as 'THN' for thin, 'FLT' for flat, 'WPY' for wispy, 'RDD' for rounded, and 'MTL' for multilevel. A '1' denotes the individual SR type, and for each multilevel SRs, an 'x' denotes the types of the stacked individual SRs.

ID	LAT	LONG	ELEV	UNIT[a]	NETWORK	CR	FAN	THN	RDD	WPY	FLT	MTL
Area01	−2.9	152.0	−2400	Apk	Isolated			1				
Area02	−0.1	142.4	−2715	Aps	Isolated			1				
Area03_A	0.2	142.0	−2730	Aml	Sub-parallel			1				
Area03_B	−0.2	142.1	−2690	Aps	Sub-parallel			1				
Area03_C	−1.3	142.0	−2705	Aps	Isolated			1				
Area04	2.1	152.8	−2580	Aml	Random					1		
Area05	1.7	149.4	−2600	Aml	Sub-parallel			1				

Table 1 (continued)

ID	LAT	LONG	ELEV	UNIT[a]	NETWORK	CR	FAN	THN	RDD	WPY	FLT	MTL
Area06_A	0.1	146.6	−2400	Ac	Branched	x		1				
Area06_C	−0.2	146.4	−2350	Ac	Branched	x	x	x			x	1
Area06_D	−0.3	146.4	−2255	Ac	Branched	x				1		
Area06_E	−0.4	146.5	−2150	Ac	Sub-parallel	x		1				
Area07_A	−1.8	156.0	−2510	Amm	Isolated			1				
Area07_B	−2.0	156.0	−2420	Amm	Branched					1		
Area08	−5.3	141.7	−3140	Npl2	Branched					1		
Area09	−5.0	141.4	−2950	Npl2	Sub-parallel					1		
Area10_A	1.3	148.7	−2500	Aml	Branched					1		
Area10_B	0.8	148.6	−2550	Aml	Isolated				1			
Area10_C	0.1	148.5	−2610	Aml	Isolated			1				
Area11	1.8	148.4	−2620	Aml	Branched					1		
Area12	0.4	147.8	−2650	Aml	Sub-parallel	x		1				
Area13_A	−3.4	151.1	−2430	Apk	Branched	x		1				
Area13_C	−3.4	151.3	−2750	Apk	Branched	x					1	
Area13_D	−3.5	151.1	−2520	Apk	Random			1				
Area13_E	−3.8	151.2	−2510	Apk	Random			1				
Area14	−2.2	151.0	−2460	Apk	Isolated				1			
Area15	0.9	150.0	−2450	Aml	Sub-parallel			1				
Area16_A	0.1	149.3	−2555	Aml	Isolated	x					1	
Area16_B	−0.3	149.2	−2530	Aml	Branched					1		
Area16_C	−0.4	149.1	−2515	Aml	Isolated				1			
Area17_A	−0.9	149.0	−2495	Aml	Isolated				1			
Area17_B	−1.0	149.1	−2495	Aml	Random					1		
Area18_B	−1.2	148.7	−2480	Aml	Branched		x			1		
Area19_A	−3.4	150.7	−2375	Apk	Sub-parallel					1		
Area19_B	−3.5	150.5	−2375	Apk	Branched			x		x	x	1
Area19_C	−3.7	150.6	−2375	Apk	Branched			1				
Area19_D	−4.3	150.5	−2400	Apk	Sub-parallel			x		x	x	1
Area19_E	−4.7	150.5	−2240	Apk	Isolated						1	
Area19_F	−4.9	150.3	−2300	Apk	Branched			x			x	1
Area20	−4.5	147.7	−1875	Aml	Sub-parallel					1		
Area21	−6.6	144.7	−1500	Npl2	Random					1		
Area22	−8.0	150.6	−850	Npl1	Isolated						1	
Area23_A	−7.6	150.2	−1920	Aml	Isolated						1	
Area23_B	−7.1	150.2	−2825	Aml	Random			x			x	1
Area24	−7.3	144.9	−1380	Npl2	Branched			1				
Area25_A	−7.1	145.5	−960	Npl2	Branched			1				
Area25_B	−6.7	145.7	−1010	Npl2	Sub-parallel	x		1				
Area26	4.8	155.2	−2680	Apk	Isolated						1	
Area27	−1.9	151.6	−2350	Aml	Sub-parallel						1	
Area28_A	−3.7	153.0	−2200	Aml	Branched			x			x	1
Area28_B	−3.9	153.1	−2085	Aml	Sub-parallel						1	
Area28_C	−4.0	153.2	−2110	Aml	Random			1				
Area28_D	−3.9	153.2	−2100	Aml	Sub-parallel	x		1				
Area29	−3.4	153.6	−2400	Aml	Branched						1	
Area30_A	−3.0	154.0	−2150	Amm	Branched			1				
Area30_B	−3.2	154.0	−2100	Amm	Branched			1				
Area30_C	−3.2	153.9	−2290	Amm	Branched			1				
Area30_D	−3.6	154.0	−2075	Amm	Branched			1				
Area30_E	−3.7	153.9	−1960	Amm	Branched			1				
Area30_F	−4.0	153.8	−2055	Amm	Branched			1				
Area31_A	−4.6	151.3	−2500	Apk	Isolated			1				
Area31_B	−4.7	151.4	−2530	Apk	Isolated						1	
Area31_C	−4.8	151.3	−2400	Apk	Isolated			1				
Area31_D	−5.0	151.2	−2500	Apk	Sub-parallel						1	
Area31_E	−5.0	151.4	−2500	Apk	Branched	x					1	
Area31_F	−5.2	151.3	−2520	Apk	Sub-parallel						1	
Area31_I	−5.4	151.2	−2390	Apk	Sub-parallel			1				
Area32	−5.8	147.3	−2000	Aml	Sub-parallel						1	
Area33_A	−5.7	154.7	−2250	Amm	Branched	x					1	
Area33_B	−6.0	154.8	−2450	Amm	Sub-parallel	x					1	
Area34_A	−4.7	154.4	−2200	Aml	Sub-parallel						1	
Area34_B	−5.0	154.6	−2300	Aml	Random					x	x	1
Area34_C	−5.6	154.3	−2350	Aml	Sub-parallel	x		x		x	x	1
Area34_D	−6.3	154.1	−2200	Apk	Branched	x					1	
Area34_E	−6.7	154.1	−2100	Apk	Sub-parallel						1	
Area34_F	−7.1	154.3	−2000	Apk	Isolated			1				
Area35_A	−4.5	154.9	−2270	Aml	Branched			1				
Area35_B	−4.6	154.8	−2300	Aml	Branched		*				1	
Area35_C	−4.7	155.0	−2500	Aml	Sub-parallel			x			x	1
Area35_D	−4.7	154.9	−2240	Aml	Branched		*				1	
Area35_E	−4.9	154.9	−2350	Aml	Branched			x			x	1
Area35_F	−5.1	154.7	−2410	Aml	Sub-parallel						1	
Area35_G	−4.6	155.2	−2300	Aml	Branched			x		x	x	1
Area35_H	−4.8	155.3	−2240	Aml	Branched			x			x	1

Table 1 (*continued*)

ID	LAT	LONG	ELEV	UNIT[a]	NETWORK	CR	FAN	THN	RDD	WPY	FLT	MTL
Area35_I	−5.1	155.3	−2190	Aml	Sub-parallel	x		x			x	1
Area35_K	−5.4	155.4	−2210	Aml	Sub-parallel	x					1	
Area36_B	−5.5	148.8	−1800	Aml	Sub-parallel			1				
Area36_C	−5.7	148.8	−1680	Aml	Branched			1				
Area36_D	−6.2	149.1	−2120	Aml	Branched						1	
Area36_E	−6.5	148.9	−2050	Aml	Branched			1				
Area36_F	−5.8	148.6	−1780	Aml	Isolated			1				
Area36_G	−5.9	148.9	−1910	Aml	Isolated			x			x	1
Area36_HI	−6.1	149.5	−1750	Aml	Branched			x			x	1
Area36_J	−6.3	149.4	−1950	Aml	Sub-parallel						1	
Area36_K	−6.4	149.5	−1950	Aml	Random					1		
Area37	−6.2	145.4	−1950	Aml	Isolated		x		1			
Area38_B	−3.2	151.8	−2375	Apk	Random			1				
Area38_C	−3.8	151.8	−2480	Apk	Isolated				1			
Area38_D	−3.9	151.7	−2515	Apk	Random					1		
Area39_A	−6.0	153.6	−2330	Apk	Sub-parallel			x			x	1
Area39_B	−6.1	153.6	−2260	Apk	Branched						1	
Area39_C	−6.2	153.6	−2160	Apk	Isolated			1				
Area39_D	−6.4	153.5	−2100	Apk	Sub-parallel						1	
Area39_E	−6.5	153.5	−2040	Apk	Branched	x					1	
Area39_F	−6.4	153.7	−2060	Apk	Branched			x			x	1
Area40_A	−4.6	153.4	−2330	Apk	Sub-parallel	x					1	
Area40_B	−5.3	153.4	−2400	Apk	Isolated			1				
Area40_C	−5.3	153.3	−2300	Apk	Isolated			x			x	1
Area40_D	−5.6	153.3	−2350	Apk	Isolated			1				
Area40_E	−5.8	153.3	−2330	Apk	Sub-parallel	x					1	
Area40_F	−5.6	153.2	−2215	Apk	Sub-parallel	x					1	
Area40_G	−6.6	153.1	−2100	Apk	Sub-parallel			x			x	1
Area40_H	−7.1	153.1	−2100	Apk	Branched						1	
Area41_A	−5.7	152.7	−2130	Aml	Isolated			1				
Area41_B	−6.1	152.7	−2100	Aml	Sub-parallel						1	
Area41_E	−6.3	152.6	−2150	Aml	Branched						1	
Area41_C	−6.5	152.5	−2000	Aml	Sub-parallel	x					1	
Area41_D	−7.0	152.5	−1900	Aml	Branched			x			x	1
Area42_A	−6.3	151.0	−1860	Aml	Branched						1	
Area42_B	−6.4	151.1	−1900	Aml	Isolated						1	
Area42_C	−6.7	151.0	−2040	Aml	Random					1		
Area42_D	−6.9	151.1	−2180	Aml	Branched						1	
Area43_A	−5.3	151.5	−2500	Apk	Branched			x			x	1
Area43_B	−5.8	151.5	−2160	Apk	Branched			x			x	1
Area43_C	−6.2	151.6	−1790	Apk	Branched			1				
Area43_D	−6.3	151.5	−1800	Apk	Branched						1	
Area43_E	−6.5	151.5	−1880	Apk	Branched						1	
Area43_F	−6.6	152.8	−1860	Apk	Sub-parallel						1	
Area43_G	−5.9	152.1	−2220	Apk	Branched			1				
Area43_H	−6.1	152.1	−1700	Apk	Isolated			x			x	1
Area43_I	−6.9	151.9	−1900	Apk	Branched						1	
Area43_J	−6.7	152.1	−1650	Apk	Branched						1	
Area43_K	−6.3	151.7	−1750	Apk	Sub-parallel						1	
Area44_A	−3.3	152.4	−2370	Apk	Random			1				
Area44_B	−3.5	152.5	−2350	Apk	Branched			1				
Area44_C	−4.9	152.1	−2500	Apk	Isolated				1			
Area44_D	−5.4	152.1	−2480	Apk	Isolated			1				
Area44_E	−4.1	152.2	−2500	Apk	Random					1		
Area45_A	−1.4	149.4	−2460	Aml	Isolated				1			
Area45_C	−1.8	149.5	−2450	Aml	Isolated		x	1				
Area45_D	−1.4	149.3	−2490	Aml	Random					1		
Area45_E	−2.0	149.3	−2400	Aml	Branched			1				
Area45_F	−2.0	149.2	−2400	Aml	Branched						1	
Area45_G	−2.2	149.4	−2400	Aml	Sub-parallel			x			x	1
Area45_H	−2.3	149.0	−2350	Aml	Sub-parallel						1	
Area45_I	−2.5	149.3	−2380	Aml	Branched						1	
Area45_J	−2.6	149.3	−2280	Aml	Branched						1	
Area45_K	−2.6	149.9	−2500	Aml	Branched			x			x	1
Area45_L	−2.8	149.5	−2250	Aml	Branched		x	1				
Area45_M	−2.8	149.6	−2280	Aml	Branched		x	1				
Area45_N	−3.1	149.7	−2380	Aml	Branched		*	1				
Area45_O	−3.1	149.8	−2410	Aml	Branched		*	1				
Area45_P	−2.2	149.0	−2300	Aml	Random			x			x	1
Area45_Q	−3.1	149.8	−2410	Aml	Branched		x			1		
					TOTALS[b]	22	7	52	7	19	47	27

[a] From Greeley and Guest (1987), using THEMIS visible images for orientation and confirmation at the large scale. Explanation of stratigraphic unit abbreviations: Aml—Medusae Fossae Formation, Amazonian lower member; Amm—Medusae Fossae Formation, Amazonian middle member; Aps—Amazonian smooth plains material; Apk—Amazonian knobby plains material; Ac—Amazonian crater material (from Tanaka et al., 1992); Npl1—Noachian cratered plateau unit; Npl2—Noachian subdued cratered plateau unit.

[b] Totals do not include the component parts of multilevel SRs.

Table 2
Percentages of SRs for individual and network classification. The most prominent percentages in each type are in bold.

	Thin	Rounded	Wispy	Flat	Multilevel	Total
Isolated	**10**%	**5**%	0%	5%	2%	22%
Sub-parallel	7%	0%	2%	**13**%	5%	27%
Branched	**14**%	0%	**6**%	12%	9%	**41**%
Random	3%	0%	**5**%	0%	2%	10%
Total	**34**%	5%	13%	**30**%	18%	100%

martian case the eroded deposits are likely part of the MFF). This erosion is commonly accomplished by aeolian and/or fluvial processes, occasioned by a change in base level or changing climate/environmental conditions. The result of this removal of the surrounding terrain is the channel floor left in positive relief (see Pain and Ollier, 1995). Fluvial channels that transition between negative and positive relief can result from localized induration and/or erosion. Continuity of inverted relief with normal relief can occur with landscape inversion in either the upstream or downstream portion of the fluvial system (Pain and Ollier, 1995).
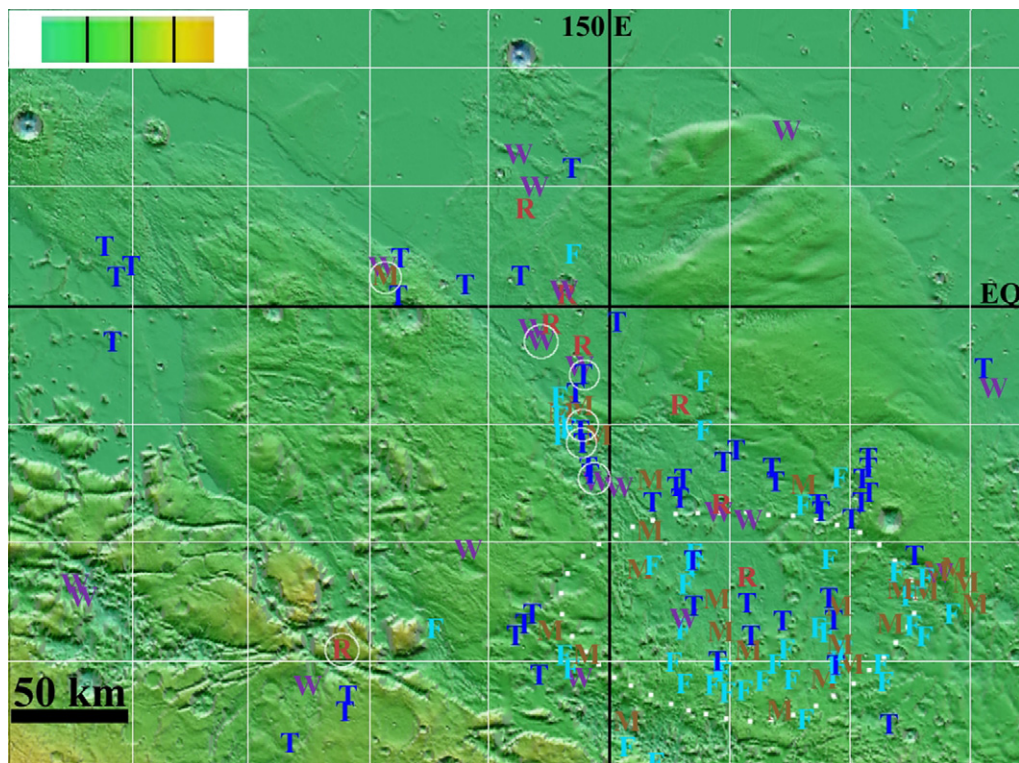
Fig. 9. Shaded relief MOLA topography with illumination from the north overlain by color MOLA topography; color bar denotes elevations from −3000 m (blue) to 1000 m (orange) in 1000-m increments. Letters indicate individual types of SR: dark blue 'T' indicates thin; light blue 'F' indicates flat; purple 'W' indicates wispy; red 'R' indicates rounded; and brown 'M' indicates multilevel. White circles surround SRs that are connected to fan or delta forms. The black rectangle shows the location of Fig. 14a. The white dots show the location of the broadly circular depression mentioned in Section 3.3.2. The black grid lines are at the equator and 150° E; the white grid lines are every 2 degrees.

Fig. 10. Oblique aerial photograph of inverted fluvial channels in Utah, western USA. Unpaved road at lower left suggests scale. The form is mainly flat topped and steep sided. However, removal of the indurated surface results in more rounded morphology in short reaches (indicated by arrows). For additional images of inverted fluvial channels on Earth, see Williams et al. (2007). In this image, illumination is from the right.
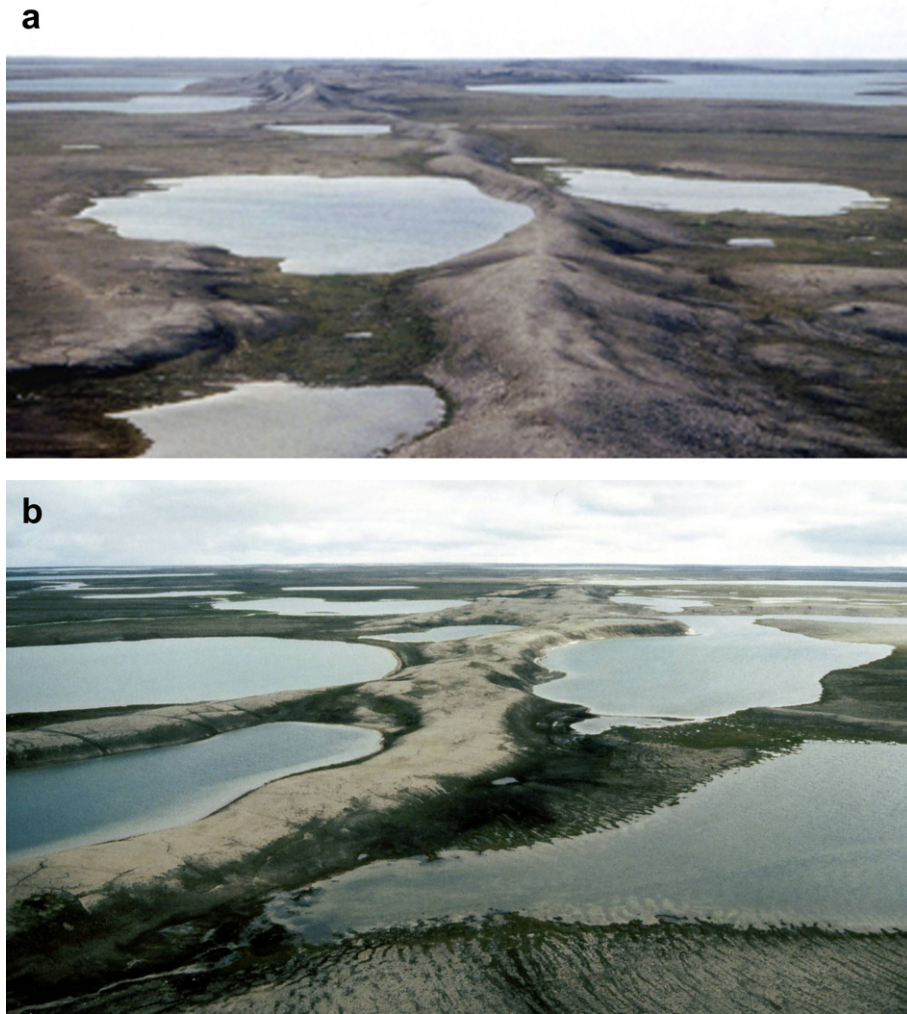
Fig. 11. Oblique aerial photographs of eskers on Victoria Island, Nunavut Territory, Canada. Note broader rounded crest in (a) and narrower rounded crest in (b). Both eskers are a few hundred meters wide.

On Earth, examples of inverted fluvial channels are found in the United States (e.g., Fig. 10) (Williams et al., 2007; Reeves, 1983; Niem, 1974; Orr and Orr, 2000), Australia (e.g., Pain and Ollier, 1995; Mann and Horowitz, 1979), Africa (King, 1942; Butzer and Hansen, 1968), and the Middle East (Maizels, 1983, 1987, 1990; Holm, 1960). For Mars, Rhodes (1980, 1981) presented an early discussion of possible landscape exhumation and inversion, suggesting that sinuous ridges in the Mangala region could be inverted fluvial channels. Howard (1981) hypothesized the existence of inverted fluvial channels in the Dorsa Argentia region, although he interpreted most of those ridges to be eskers. Subsequently, Williams and Edgett (2005) observed that some SRs have continuity relationships with traditional valley networks, evidence in support of a fluvial origin for those SRs. The preservation of fluvial networks on Mars is complex, with some channels that are filled and buried, others that have discontinuous preservation, and still others that are preserved in inverted relief (Williams and Edgett, 2005; Edgett, 2005). SRs interpreted to be inverted fluvial channels are at various locations around the planet, including Arabia Terra, Lunae Planum, and within crater basins such as Eberswalde (Mangold et al., 2004; Malin and Edgett, 2003; Moore et al., 2003; Williams et al., 2005; Williams, 2007). One of the branched SR networks shown here (Fig. 2b) was hypothesized to be fluvial by Irwin et al. (2005), Williams and Edgett (2005), and McMenamin and McGill (2005).

3.2.2. Eskers

Glaciofluvial ridges may form from sedimentation in ice-walled meltwater channels associated with glaciers (Banerjee and McDonald, 1975). Such meltwater channel fills may occur in supraglacial channels, in englacial or subglacial conduits, or within ice-walled canyons near the glacier margin, provided there is adequate sediment supply. Melting of the supporting ice (channel boundary) associated with warming climates leaves sinuous sedimentary ridges, or eskers (Fig. 11) (see Brennand, 2000 for a review of esker formation mechanisms). The excellent preservation of the ridge form of most eskers associated with past ice sheets suggests that they were likely formed in subglacial or near-bed englacial conduits or in ice-walled canyons near the glacier margin; ridge form preservation is not favored by differential ablation and let-down of supraglacial or near-surface englacial channel fills (Brennand, 2000). Eskers may alternate co-linearly with valleys of similar width to the esker. The implication in such an instance is that the conduit likely varied in width along its length, resulting in varying velocity (at constant discharge) and causing fill in reaches with large width and erosion in reaches with small width. Eskers may also terminate in sub-aerial or subaqueous fans or deltas, and occur within larger valleys (tunnel valleys). They occur on negative slopes (where water flow was down-gradient) and on positive slopes (where water flow was up-gradient). Terrestrial eskers are found in association with other glacial landforms such as drumlins and moraines.

On Earth, examples of eskers are found in formerly glaciated regions such as Canada (e.g., Brennand, 2000) (Fig. 11) and the northern United States, Scandinavia (e.g., Hebrand and Åmark, 1989), and Ireland (e.g., Knight, 2002). On Mars, eskers have been hypothesized to explain SRs in the Argyre and Hellas Planitiae (Kargel and Strom, 1992), the northern plains (e.g., Kargel et al., 1995; Kolb and Tanaka, 2001) and the polar regions (Howard, 1981; Fishbaugh and Head, 2001; Head and Pratt, 2001). Some of the SRs mapped here were hypothesized to be eskers by Nussbaumer et al. (2003) and Kite (2004). Nussbaumer et al. (2003) suggested that the sharp bends in the SR shown in Fig. 2a were indicative of concertina eskers, which form during glacial surging (Knudsen, 1995).

3.3. Origins of selected types of SRs

The SRs appear to be only partially preserved and/or partially revealed by MFF erosion, inferred to be mainly aeolian on the basis of prevalent yardangs. In addition, the lack of fine stratigraphic markers in the western MFF, along with the low density of Mars Orbiter Laser Altimeter (MOLA) data in this equatorial region, makes the stratigraphic positions and relationships of SRs ambiguous. Within these limitations, consideration of SR types and landform associations form the basis for inferring their mode of formation.

3.3.1. Flat or multilevel SRs in branched or sub-parallel networks

The large majority of flat SRs are located in areas of regional erosion, namely, along the interior edges of the MFF lobes or along the scarp adjacent to the Aeolis Planum highlands, suggesting that they have been exposed by this erosion. In addition, the morphology of flat SRs suggests that they are composed of more resistant material that has eroded out of a volume of less resistant material. These SRs have flat upper surfaces with steep side slopes that transition abruptly to the surrounding terrain. This sharp-edged appearance indicates that these SRs are composed of material that is resistant to weathering or disintegration. As noted above (Section 2.1.4), a single flat SR is located on Cerberus Palus (Fig. 5d), inferred to be the site of lava emplacement (Keszthelyi et al., 2000, 2004; Plescia, 2003).

That flat SRs are often associated with scarps (e.g., Fig. 7) suggests that the local terrain is backwearing. The tens-of-meters-high edges of the SRs indicate that downwearing may also be contributing to SR exposure. In some cases, flat SRs can be seen to transition from continuous features into curved lines of disjointed, adjacent knobs (e.g., Fig. 5a). Because of their co-linearity with other flat SRs and their curvilinear plan-view morphology, we infer these knobs to be the result of advanced aeolian erosion of flat SRs. The discrete, high-relief shape of the knobs, some of which maintain their flat-topped morphology, also implies erosion of a cohesive, indurated, or resistant substrate. The single flat SR on Cerberus Palus is noteworthy because it appears to transition from positive to negative relief, although the local junction at the ridge-trough transition is enigmatic. A similar transition was pointed out by Williams and Edgett (2005) in Arabia Terra, where it was interpreted as indicating SR formation by fluvial channel inversion. On Earth, alternating ridges and troughs (valleys) have also been ascribed to glaciofluvial processes, where the ridge is a subglacial conduit fill (esker) and the valley is erosional (e.g., Shetsen, 1987). Given the geologic context of this SR within the lava-filled Cerberus plains, a more likely explanation for this single flat SR may be as a lava channel that has become 'perched' through lava overflow.

The result of comparison of the global THEMIS night time IR mosaic available at http://jmars.asu.edu/data/ and SRs in THEMIS visible wavelength data is commonly though not universally consistent with SR formation as strongly cohesive or indurated material eroded from less resistant material. That is, many of the large SR networks (for example, parts of Area43) are visible as relatively brighter sinuous features compared with relative darker surroundings in the night time IR mosaic. This relative brightness suggests that they are comprised of relatively higher thermal inertia material. This higher thermal inertia, in turn, may be reasonably attributed to cohesion of sediments, indurated material, or coarse-grained material resistant to erosion. However, this result is not uniform, as not all SR networks are visible in the night time IR data, even in cases where their spatial extent is larger than the data pixel size (for example, Area35). That the preponderance of SR networks is visible in night time IR data generally supports their formation as resulting from erosion, but further investigation is required to quantify the extent of SRs visibility in night time IR data and its implications.

Fluvial channel inversion requires some form of erosional resistance or greater hardness relative to the channel surroundings, whereas esker formation does not. Therefore, the inference that these flat SRs are more resistant to erosion than the surrounding terrain supports their formation as inverted fluvial channels. The flat-topped morphology, which is the most common morphology observed for inverted fluvial channels in Utah (Williams et al., 2007), is consistent with their formation as inverted channels. Most (83%; see Table 2) flat SRs have either a branched or sub-parallel network pattern. These network patterns commonly characterize fluvial networks (e.g., Howard, 1967), supporting the interpretation of flat SRs in branched or sub-parallel networks as inverted fluvial channels.

The lowest levels of multilevel SRs always have flat morphology, although they may lack distinct edges or steep side slopes. Like flat SRs, multilevel SRs are commonly associated with scarps, and most multilevel SRs (Table 2) also have branched or sub-parallel networks. Because of their morphological, contextual, and network similarity to flat SRs, we hypothesize that steep-sided, multilevel SRs are also a result of exposure of indurated materials by backwearing and/or downwearing of the surrounding volume of material. The superposition and colinearity of the upper and lower ridges, even where they branch and loop (e.g., Fig. 5a), indicate that the superposed ridges making up multilevel SRs are genetically related. The observed plan-view morphology bears a qualitative resemblance to the floodplains simulated by meander models (e.g., Howard, 1991, 1996; Sun et al., 2001). Thus, the lower, flat SRs may reasonably represent a sedimentary unit that was deposited across a floodplain by a meandering channel and is now resistant to erosion, due either to cementation or to clast armoring. In this scenario, the upper, thin SRs would have formed through inversion of narrow fluvial channels set in a less resistant sedimentary substrate on top of the lower, flat SRs that formed through inversion of floodplains.

Finer-scale details—specifically, the narrow, semi-concentric or sub-parallel, curved ridges on flat and multilevel SRs (Figs. 5b and 5c)—support this interpretation of flat/multilevel SRs as inverted floodplains. These fine-scale, curved ridges appear similar to meander scars or scroll bars seen on terrestrial meandering river floodplains (Leopold et al., 1992; Knighton, 1998) (Fig. 12). In fluvial geomorphology, meandering is both a channel pattern and a process by which a river migrates laterally with respect to the down flow direction. Meandering is an effect of the differential erosion produced by the helicoidal (screw-like) flow in a river. The faster flow on the outside of channel bends causes greater erosion than does the slower flow on the inside of the channel bends. This greater erosion on the outside of the bends is approximately matched by deposition on the inside of the bends, usually in the
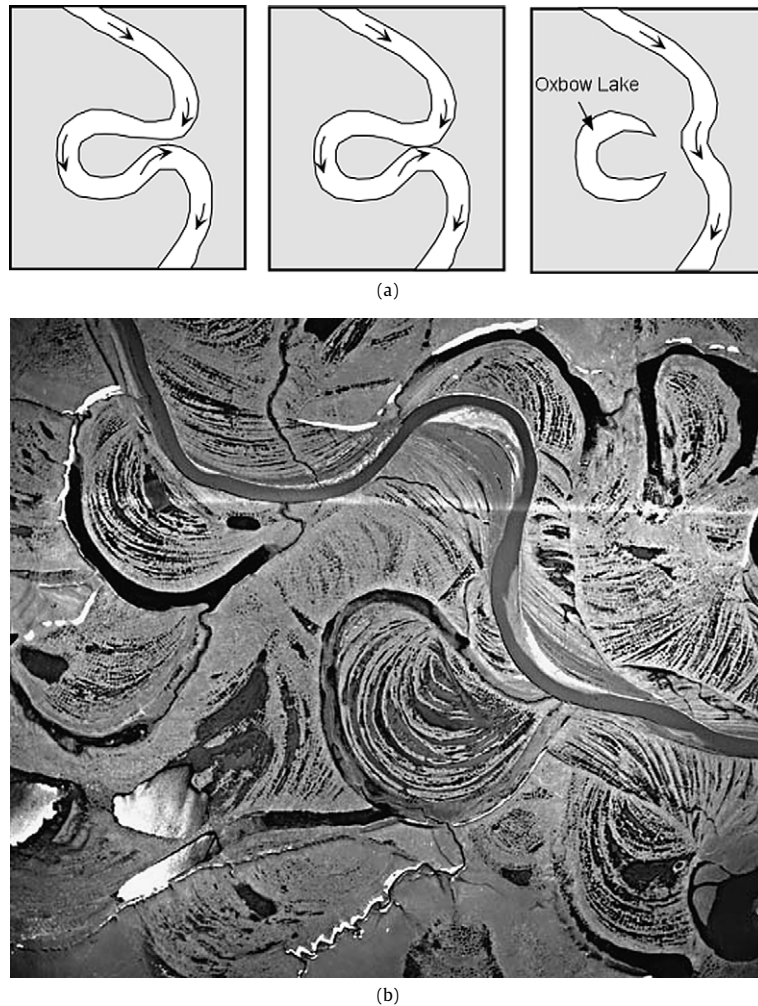
(a)

(b)

Fig. 12. (a) Cartoon showing increasing meander wavelength, terminating in meander neck cut-off and formation of an ox-bow lake. (b) Scrolled floodplains in Alaska (from Geomorphology from Space, http://geoinfo.amu.edu.pl/wpk/geos/GEO_HOME_PAGE.html).

form of a point bar. Point bars often have medial ridges produced by deposition on the bar during flood stage in combination with erosion behind (shoreward of) the bar during low flow. Because meandering enhances helicoidal flow, meander amplitude tends to increase with time. This increase in meander amplitude produces a series of sub-parallel, semi-concentric point bar ridges (scroll bars) delineating the past positions of the river as it migrated across the floodplain. Eventually, a meander loop may become so goose-necked (sinuous) that the river cuts through the meander neck, creating an ox-bow lake (Fig. 12a). The resultant landform is a floodplain with scroll bars (curved swaley topography) and oxbow lakes (arcuate lakes) (Fig. 12b) (Leopold et al., 1992; Knighton, 1998).

The morphology observed on the surface of flat SRs and the subjacent level of multilevel SRs is similar to that of scrolled floodplains, namely, a series of sub-parallel, fine-scale ridges that form roughly symmetrical, semi-concentric loops. Their size of order 10^2–10^3 meters in amplitude is similar to that of terrestrial scroll bars or meander loops. They also appear to have topographically higher outer edges than inner edges, as are produced by terrestrial meandering rivers, although this appearance has not been confirmed with high resolution topography. If flat SRs and the subjacent levels of multilevel SRs are formed as scrolled floodplains, the following sequence of events is implied (see Fig. 13):

(1) An actively meandering river deposits point bars on the insides of meander bends. As the river migrates, point bar formation and accretion leaves scroll bars in the floodplain. The surface of the floodplain is composed of fluvial sediments deposited by the meandering river.

(2) Over time, the river dries up and the channel fills with sediment. The entire floodplain including the infilled channel becomes indurated.

For flat SRs:

(3) Regional scale erosion preferentially removes the less resistant (non-indurated) surrounding sedimentary material. This preferential removal leaves the indurated floodplain with scroll-bar topography in inverted relief. The result is a flat SR.

For multilevel SRs:

(3) Sediments are deposited on top of the indurated floodplain. Some type of environmental or geophysical trigger (e.g., atmospheric, hydrologic) creates a river within these deposited sediments.

(4) With additional environmental or geophysical change (e.g., climatic, seasonal), the river dries up and its bed is more resistant to erosion than the surrounding floodplain. This greater
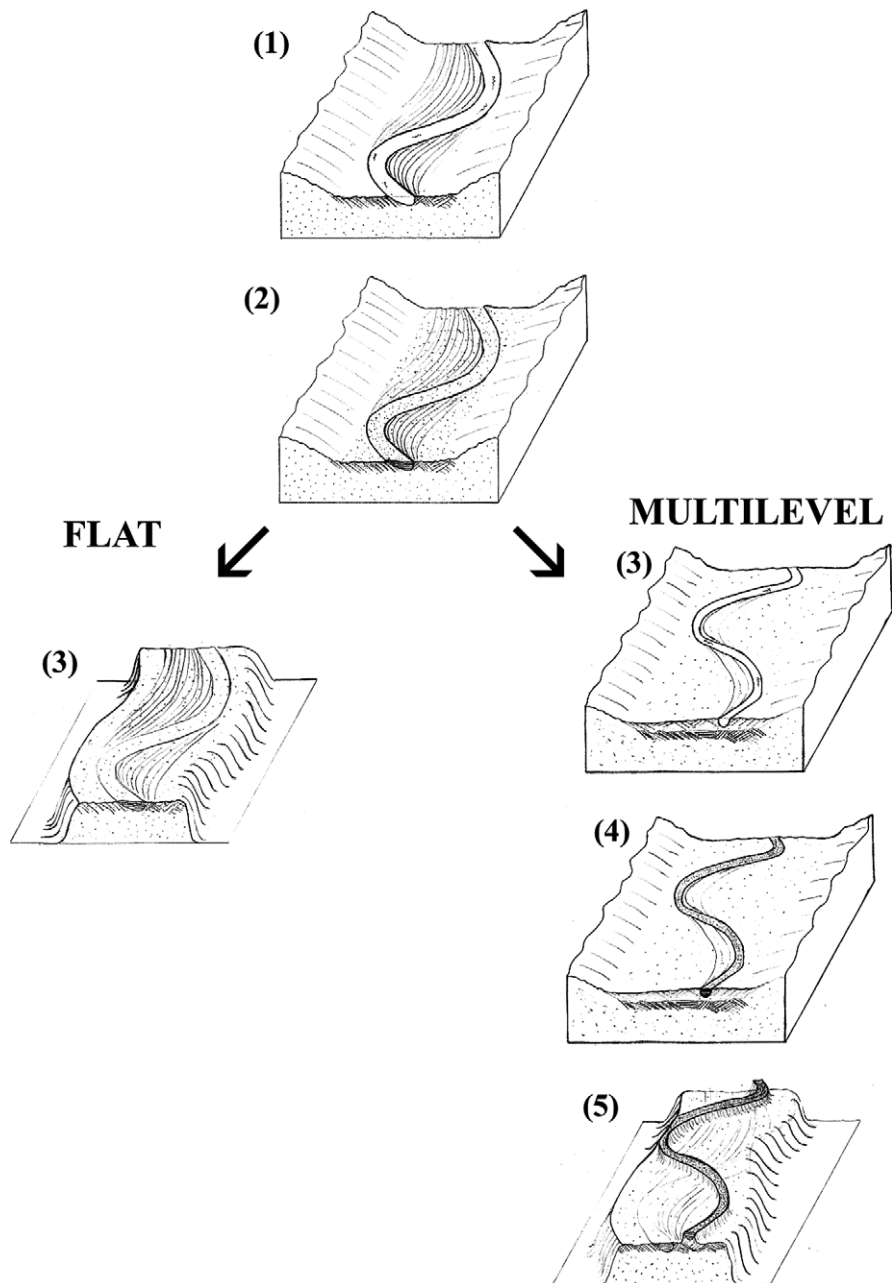
Fig. 13. Cartoon showing the proposed sequence of events leading to flat (on left) and multilevel (on right) SRs. Darker shading indicates greater induration. See text for description of each stage.

resistance in the river bed could be due to deposition of a boulder lag, infill by lava, or chemical cementation.

(5) Erosion of the less resistant surrounding sediments produces an inverted channel on top of the inverted floodplain with scroll-bar topography. The result is a multilevel SR.

The proposed explanation for the sub-parallel, semi-concentric curves as fluvial meander bends is our preferred hypothesis. However, the origin of other inferred meander bends on Mars, namely those in Eberswalde Delta, Holden NE crater (Malin and Edgett, 2003; Moore et al., 2003; Wood, 2006; Jerolmack et al., 2004) has recently been called into question, because the meander loop topography, color alternations, and asymmetric bends are held to be atypical of terrestrial fluvial meanders (Fedo et al., 2007; Kraal and Postma, 2008). The suggested formation of these flat or multilevel SRs with sub-parallel, semi-concentric curves as scrolled

floodplains requires additional testing as one of multiple working hypotheses.

3.3.2. Rounded (and thin, sharp-crested) isolated SRs

In contrast to flat SRs, rounded SRs have a smooth topographic cross-section with side slopes that grade gently into the surrounding terrain (Fig. 3). This appearance suggests that rounded SRs formed by loose sedimentation rather than by induration and subsequent differential erosion. For inverted fluvial channels in Utah where the indurated capping layer is being eroded (Williams et al., 2007), stretches with rounded morphology tend to be short and discontinuous (e.g., Fig. 10), whereas the rounded SRs on Mars extend for several tens of kilometers. This suggestion of loose sedimentary composition over indurated fine material is supported by a lack of aeolian erosive morphology for rounded SRs. That is, none of the rounded SRs transition into disjointed knobs, as

do several of the flat SRs. These indications of formation by loose sedimentation are most consistent with formation as eskers. In eskers, granular sediment collapse associated with the removal of ice support will have the tendency to produce rounded crests, more gentle side slopes, and more gradual slope angle transitions with surrounding terrain (Fig. 11), than are expected from the formation of inverted fluvial channels with indurated river beds (Fig. 10) or floodplains. Rounded morphology is thus consistent with an esker inference (Brennand, 2000).

The most diagnostic characteristic distinguishing eskers from inverted fluvial channels is irregular change or increase in ridge elevation in the down flow direction. Fluvial channels decrease in elevation in the down flow direction because unpressurized water flow is controlled by gravity; consequently, rivers flow downhill. Flow in subglacial conduits, however, is controlled by the potentiometric surface that is a result of the topography of the land, the pressure of the overlying ice, and the water flux (Röthlisberger, 1972; Shreve, 1985). As a result, eskers that form in subglacial conduits can have upslope paths and may cross topographic divides, although the increased flow pressure at such locations generally precludes deposition of sediment, causing esker discontinuity (Shreve, 1985). Given the ratio of water to ice density, and assuming steady state conditions, the maximum slope on which an esker can form is approximately 9°, although post-formation tectonic or glacioisostatic adjustments can change the observed slope from its original value (e.g., Brennand, 1994).

To investigate the possibility that rounded SRs are eskers, we used MOLA data to analyze the regional and local slopes of rounded SRs in the low area between the MFF lobes. THEMIS visible image coverage does not show the connections among these SRs, and we have recorded them as three individual features (Area14, 38_C, and 44_C) in Table 1. However, the global THEMIS day IR mosaic available at http://jmars.asu.edu/data/ suggests that they are a single feature (Fig. 14a). In order to measure the regional slope over the longest possible extent, we have plotted MOLA data over all three rounded SRs, which includes the northern part of Area44_C, all of Area38_C, and all of Area14. Individual MOLA data points cover roughly 170 m on the Martian surface, typically separated by 300 m from neighboring data points (Zuber et al., 1992; Smith et al., 1998). Our MOLA data was gridded at ∼0.5 km/px, although between-track spacing in this equatorial region was as wide as a few kilometers.

Regionally, the gridded (Fig. 14b) and individual (Fig. 14c) MOLA data both show this north-south oriented chain of rounded SRs to be higher in the north and lower in the south. The total elevation difference is ∼100 m over a distance of ∼250 km, which equals a gradient of 0.023°. In our preliminary mapping, the flow direction is ambiguous, so whether water flow increased in elevation with distance to the north (e.g., as an esker) or decreased in elevation with distance to the south (e.g., as either a fluvial channel or an esker) is unclear. This gradient is less than the maximum upslope value for eskers. Thus, it allows for interpretation of the SR as an esker formed in a subglacial conduit within a glacier centered to the south with flow to the north. MOLA topography shows a broadly circular depression between the two western MFF lobes (Fig. 9). The past presence of a glacier at this location with extension northwestward between the two MFF lobes would explain the clustering of rounded SRs in this region (Fig. 9).

Locally, the MOLA topography provides more diagnostic evidence of formation of this chain of SRs as eskers. MOLA topography shows that the SRs cross local topographic highs, entailing elevation increases of up to ∼100 m (Table 3 and Fig. 14c). These topographic highs are local maxima, so that elevation increases regardless of the direction of flow along the SRs. Eskers may commonly cross topographic divides, whereas rivers cannot flow upslope. Thus, the profile of the SRs over these local topographic highs

Table 3
Local elevation increases along the chain of rounded SRs between the two western MFF lobes. The amount of elevation increase was estimated as the local maximum height minus the highest minimum on either side (see Fig. 14c or Fig. 14b for locations of individual topographic divides).

Distance along SR	Increase in elevation
80–140 km	∼100 m
175–200 km	∼50 m
220–250 km	∼40 m

(Figs. 14b and 14c) strongly supports their interpretation as eskers rather than inverted fluvial channels.

Other data are consistent with an esker interpretation for rounded SRs, although not uniquely so. All rounded SRs have isolated network patterns (Table 2). Dendritic esker networks (types I and IV, Brennand, 2000) typically cover large areas with 10^2–10^3 km along eskers between junctions. Other eskers form parallel networks with a typical distance of 10^1–10^2 km between eskers (type II, Brennand, 2000). Most of these esker types would appear isolated at the coverage of the THEMIS visible wavelength images. In contrast, fluvial channels commonly form in higher-density networks and when preserved as inverted channels, they may create overlapping patterns (see Williams et al., 2007, Figs. 5 and 9). However, fluvial channels may also form in isolation, so isolation is not uniquely diagnostic of formation mechanism. Even from an original network of features, partial preservation or exposure may produce an isolated SR.

The termination of a rounded SRs in a fan-shaped form (Fig. 8a) is also consistent with SR formation as an esker. Most terrestrial eskers terminate in fans or deltas (Brennand, 2000). However, rivers also terminate in fan-shaped forms so this observation is not uniquely diagnostic.

The observed rounded morphology is also consistent with either an esker or inverted channel interpretation. As discussed above, the rounded shape is common for terrestrial eskers, in which context it results from collapse of the loose sediment. However, it could also be due to advanced erosion of the indurated upper layer of inverted fluvial channels or to collapse of coarse-grained sediments where the inversion was the result of a coarse-grained lag deposit.

Finally, other characteristics of the rounded SRs are *in*consistent with formation as eskers. The pronounced sinuosity shown in Fig. 3 seems to us atypical of eskers, which do not commonly form high sinuosity meander loops. Also, definitive glacial landforms around these rounded SRs are largely lacking. This apparent lack of associated glacial landforms may be due to (1) the resolution and coverage of the images examined here, or (2) erosion of most associated (thin and less resistant) glacial deposits by wind. Yardangs frequently surround rounded SRs (e.g., Fig. 3). In the glacial landscape, eskers could have contained the coarsest sediment, and thus have been the most resistant glaciogenic landform to subsequent wind erosion.

An example of possible glacial landforms may be seen in Fig. 2a, which shows a thin SR surrounded by hummocky terrain located immediately east of the rounded SRs in Fig. 14 (see Fig. 9 for location). Hummocky terrain may form in terrestrial settings as a result of the let-down of supraglacial debris as ice melts (Gravenor and Kupsch, 1959). Immediately west of the rounded SRs in Fig. 14 is a thin SR with a sharp crest (Fig. 2c). A sharp-crested morphology characterizes some terrestrial eskers (Fig. 11b). Sharp-crested eskers may be formed due to granular sediment collapse during the melting of partially buried ice (in addition to the melting of conduit walls) (Brennand, 2000). Alternatively, such esker morphology may result from strong melting along descending or gently ascending (<1.7× the ice surface slope) reaches within steady-state subglacial conduits (Shreve, 1985). Consequently, thin, sharp-crested
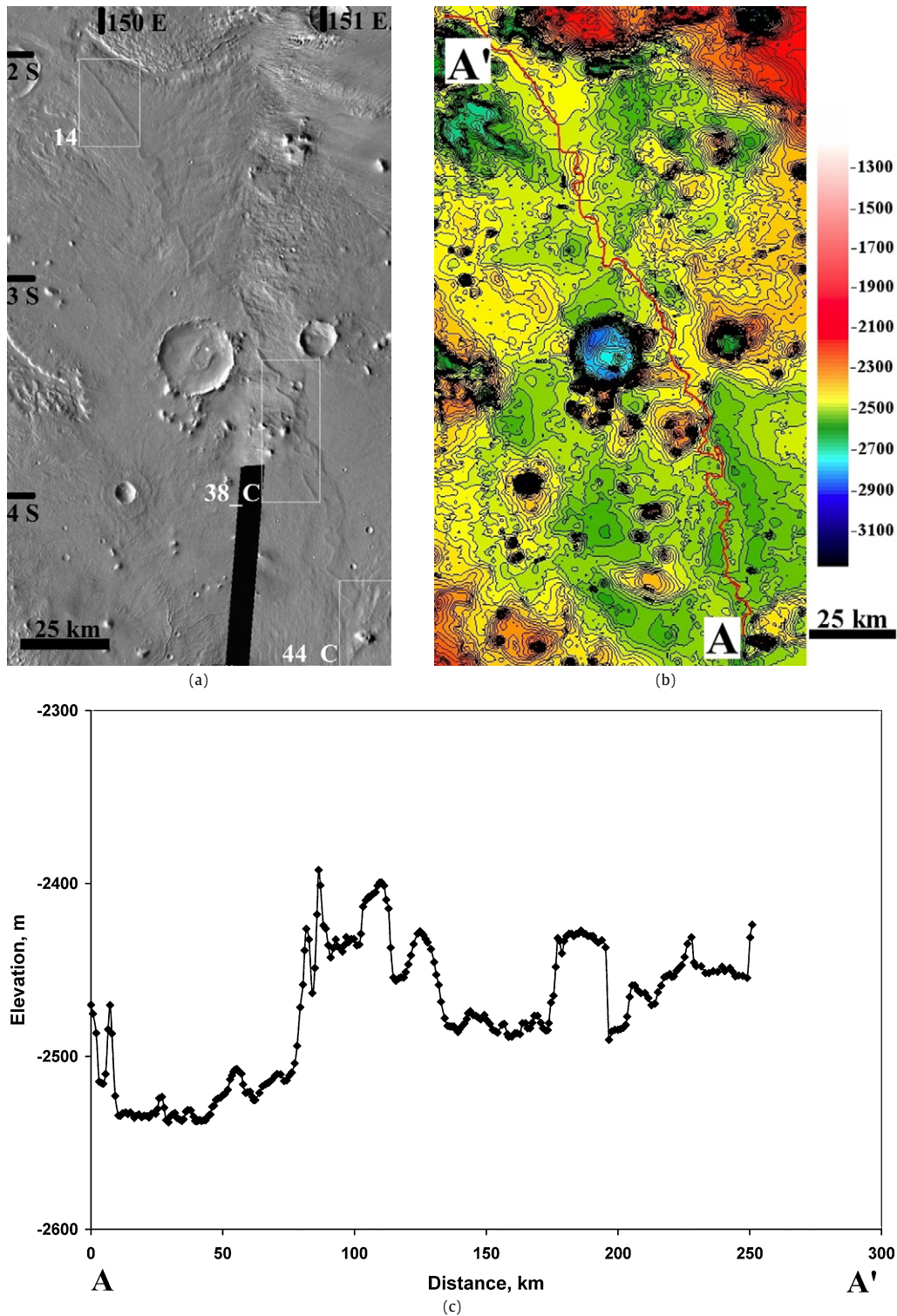
Fig. 14. Images showing rounded SRs in the broad topographic depression between the two western MFF lobes. (a) A portion of the global THEMIS day IR mosaic showing rounded SRs (black box, Fig. 9). These SRs are classified on the basis of THEMIS visible wavelength images as three isolated SRs (14, 38_C, and the northern part of 44_C), with locations shown by the white boxes. As shown here, these rounded SRs appear to be portions of the same landform. (b) Gridded and contoured MOLA topography, covering the same area as (a). The trace of the single rounded SRs inferred from (a) is denoted by the red curvy line (A–A′). The contour interval is 20 m; color scale bar is in meters. (c) Elevation profile of the rounded SR shown in (a) and outlined in (b) (A–A′). The points are defined as the 75th percentile elevation of individual MOLA data points within the 2 km radius surrounding the digitized line of points along the SR.

SRs may be eskers and the host terrain for other SRs may be glaciogenic hummocky terrain, although neither this morphologic analogy nor the interpretation of the hummocky terrain as glaciogenic is conclusive at this time.

In summary, our preferred hypothesis for the origin of rounded SRs is as subglacial conduit fills or eskers. This interpretation is impelled by the topographic data, which show stretches of locally high elevation, requiring upslope water flow, and is consistent with

the rounded individual morphology, the isolated network morphology, and the termination of SRs in fans or deltas. Sharp-crested thin SRs may also be glaciogenic, as they are morphologically similar to sharp-crested terrestrial eskers. However, the high sinuosity of the rounded SRs is atypical of terrestrial eskers, and other glacial landforms commonly associated with terrestrial eskers are not clearly evident in the images analyzed in this study, although the terrain surrounding the thin SR in Fig. 2a may be glaciogenic. An alternative hypothesis is that the rounded SRs are inverted fluvial channels, whose rounded morphology reflects inversion and gravitational collapse of a coarse grained lag. Such an unconsolidated river bed may have been coarser than the surrounding materials but less indurated or only weakly more indurated or lithified than the surrounding sediments or rock.

3.3.3. SRs associated with impact craters

Twenty-two SRs are denoted as being associated with impact craters. Over one-half of these SRs are flat, over one-quarter are thin, three are multilevel, and a single example is wispy; none is rounded (Table 1). These SRs have network patterns that are either branched (Fig. 6) or subparallel (Fig. 7), with one example having an isolated network pattern (Table 1). Modeling suggests that impact craters could generate a long-lived hydrothermal system (e.g., Barnhart et al., 2008, and references therein) and the MFF has been hypothesized to be water–ice rich (Head and Kreslavsky, 2001; Watters et al., 2007). Conceivably, these factors might produce channelized aqueous flow from impact into the MFF. However, analysis of current data does not show any evidence that any SRs were formed by the impact craters with which they are associated. To illustrate this, we present an analysis of the two examples shown in Figs. 6 and 7.

Fig. 6a (Area33) shows a branched network of flat SRs with extensive sub-parallel, semi-concentric curves (inferred scroll bar morphology) located to the northwest of a 15.5-km-diameter impact crater. This SR network overlies the fluidized ejecta of the impact crater (Fig. 6a). This stratigraphic relationship indicates that the crater predated the SR network, and that the SRs formed in an overlying, post-impact deposit. Likewise, the well-preserved appearance of the ejecta suggests that it has been exhumed from beneath a protective mantling deposit. The SRs cross the ejecta rim at local low points (Fig. 6b); a plot of MOLA track 12251 suggests that the tops of the SRs stand ~50 m above the low parts of the ejecta lobe where they cross it. This spatial coincidence indicates that the SRs were formed by gravity-driven fluid flow that exploited these topographic minima, and that the mantling unit in which they formed was thin enough to conform to the underlying ejecta topography. In MOLA track 12220, the tops of the SRs stand ~150 m above the lowest part of the exhumed crater ejecta (Fig. 6a), suggesting the removal of up to 150 m of overlying mantling deposit.

Sinuous troughs originate at the crater rim. These troughs both cross-cut and connect with SRs (Fig. 6c). This relationship indicates that the troughs formed both syngenetically and subsequently to the SRs. This conjunction of the sinuous troughs and SRs occurs around the base of the crater rim, which is marked by a small scarp (Figs. 6a and 6c). The height of this scarp, from the base of the crater rim down to the top of the SRs, provides an estimate of the thickness of the now-eroded mantle in which the SRs formed. MOLA track 12220 suggests a difference between the base of the crater rim and the SR surface of about 50 m. Given that this location is topographically higher than the surrounding terrain, this estimate is a lower bound on the mantle unit thickness. It is thus consistent with the maximum estimate of ~150 m derived for elsewhere on the ejecta blanket, and with the inference that the mantling unit in which the SRs formed was relatively thin.

In addition to sloping down and out from the crater rim, these sinuous troughs also slope down and into the crater, in one case continuing onto the crater floor as an inchoate SR (Fig. 6d). This morphology indicates bi-directional flow in the troughs, suggesting that the source of the liquid that formed them was atmospheric; this implies their formation by runoff from precipitation (either snow or rainfall). The maintenance of the observed sharp crater rims would not be likely in the presence of precipitation, but can be explained by the mass wasting of the crater rim through listric faulting, which is evidenced by the slump blocks just inside of the sharp crater rim (Fig. 6d). The absence of fault blocks inside other stretches of sharp crater rim may be due to their erosion and/or covering by transverse aeolian ridges.

These observations suggest a multi-part scenario for formation of this branched network of flat SRs: (1) an impact occurred, creating the crater and its fluidized ejecta, (2) a ~50–150 m thick mantling unit was deposited over the crater ejecta, extending up to the base of the crater rim, (3) runoff from precipitation created troughs on the exposed crater rim which fed into a branched network of meandering rivers or floodplains in the mantling unit, (4) the meandering rivers or floodplains in the mantling unit became indurated, (5) the rest of the mantling unit was eroded, leaving the branched network of rivers or floodplains as a branched network of flat SRs. After SR formation, precipitation runoff occurred or continued, causing some sinuous troughs to truncate or cross-cut some SRs. The ejecta to the southeast of the crater appear less eroded than elsewhere around the crater. In MOLA track 10672, this area stands ~240 m higher than the ejecta blanket to the north and over 100 m higher than the SRs to the northwest (Fig. 6a). Thus, this area may contain the buried headward extension of the SR network, some of which is visible beneath the crater rim on the northwest and the southeast sides of the crater (Fig. 6a). The suggestion that SRs encircle both sides of the crater beneath uneroded ejecta also weighs against a causal relationship between the SRs and the crater.

A sub-parallel network of flat SRs is also visible in the southwestern interior of the crater (Area33_B, Table 1). These channels seem to occupy multiple stratigraphic levels, although no MOLA tracks cross these SRs to assess this. No connection with the exterior branched network of flat SRs is apparent.

Fig. 7a (Area35) shows two SR networks spatially associated with two different ~2.3-km-diameter impact craters. The global THEMIS day IR mosaic shows that the individual members of the northern SR network extend and connect to the west (Fig. 7b). An immediate westward extension is not apparent for the southern network, but a limited number of degraded SRs are visible to the far west (west of the western impact crater labeled in Fig. 7b). Both networks have multiple subparallel SRs that diverge eastward.

The gridded MOLA topography shows that these craters are located on a topographic high ('western rise') between two troughs (Figs. 7b and 7c). To the far east is a scarp and an adjacent plateau ('plateau,' Figs. 7b and 7c), which stands ~250 m above the level of the SR networks. These spatial relationships show that the northern SR network, and probably the southern network as well, were likely part of a single tributary system in which water flowed from the eastern high-standing plateau westward (Fig. 7b). Even in their current state, these SR networks cover a significant area (Fig. 7b). If the eastern plateau held the headwaters of these SR networks, they must have developed before erosion formed the adjacent scarp and troughs and so must have originally extended farther to the east. The disconnected but co-linear knobs around the craters (Fig. 7a) and the degraded SRs visible to the far west (Fig. 7b) are interpreted as remnants of these earlier, now eroded SRs. Thus, the original SR network must have been considerably more extensive in all directions than in its current state. Such a broadly tributary network as shown in Fig. 7 implies a broadly

distributed water source, which is most easily provided by atmospheric precipitation (either as rainfall runoff or snowmelt). In this case, the impact craters in Fig. 7a are inferred to have formed on top of and subsequent to the formation of these previously more extensive networks with which they are spatially associated.

As these examples illustrate, current data do not provide evidence that the SRs associated with impact craters are genetically related to their associated impact craters. The SRs in Fig. 6 (Area33) formed in a mantling unit deposited after the impact, and appear to wrap around the crater. The SRs in Fig. 7 (Area35) headed on the eastern plateau, and, having formed before the impacts, are unaffected in their orientation by the craters. In either case, the relationships between the SRs and their associated craters appear to be coincidental. In both cases, SR network formation by some form of precipitation is implied.

3.3.4. SRs associated with fans or deltas

As noted in Section 2.4 above, fan-shaped forms are visible at the ends of a small number of SRs. Because of their fan-shaped plan-view morphology, their location at the termini of SRs, and their apparent decrease in elevation with distance from that point, we interpret these forms to be either alluvial fans, deltas, or subaqueous (drowned) fans.

Fans or deltas may form by sediment deposition from flowing water in either fluvial or glaciofluvial environments. In fluvial environments, fan-shaped landforms result from the deposition of sediment at the termination of a river typically either at a slope break (resulting in a subaerial or alluvial fan) or into a standing body of water (forming a subaqueous fan or delta). The nature of the depositional environment affects the resulting fan morphology. Radial ridges on alluvial fans or deltas could be caused by clast-armoring or cementation of the sediments transported in channelized flows across the fan or delta surface. Subsequent differential erosion of the entire region would result in topographic inversion of the headward fluvial channel bed into an SR as well as inversion of the radially-branching channels on the fan into ridges.

In glaciofluvial environments, eskers can also terminate in subaqueous fans or deltas and in subaerial (or alluvial) fans (Brennand, 2000). Most glaciogenic subaerial fans and deltas have only minimal textural difference over the fan surface. This homogeneous texture is due to sheetflow inundating the fan or delta surface or frequent position switching of channelized flow, processes which may also occur on river-fed fans in areas of high precipitation and topographic relief. Thus, glaciogenic subaerial fans and deltas would be unlikely to develop radial ridges. However, glaciogenic subaqueous fans often record high-energy events and rapid sedimentation (e.g., Russell and Arnott, 2003). These conditions can result in coarse-grained scour-fills (channelized traction deposits) surrounded by finer-grained suspension deposits, which are inherently more erodible if not indurated. The coarser scour fills could become radiating ridges due either to differential compaction during dewatering or to differential erosion (cf. Matile and Groom, 1987).

Thus, the observed fans with low-sinuousity, radial ridges could have formed either from fluvial or glaciofluvial processes. In this initial analysis, they do not help to discriminate between these two hypothesized formation mechanisms for SRs.

4. SR stratigraphic and topographic context

4.1. Stratigraphic context

To assess the stratigraphic context of SRs, we have used the 1:15,000,000 scale map of Greeley and Guest (1987). The 1:5,000,000 map of Tanaka et al. (1992) is of higher resolution, but only extends southward to the equator and the mapped units do

Table 4

Percentages of SRs by stratigraphic unit (based on Greeley and Guest, 1987). The most prominent percentages are in bold. Rounding error causes a total of greater than 100%. (For explanation of stratigraphic unit abbreviations, see footnote for Table 1).

Unit	Aml	Amm	Aps	Apk	Ac	Npl1	Npl2
Percentage	**48**%	7%	2%	**37**%	3%	1%	6%

not correlate well with the older, adjacent map to the south (Scott et al., 1978). Thus, we have used Greeley and Guest (1987) to derive a basic understanding of the stratigraphic units that host the SRs identified in this study. On-going mapping of this region will likely improve or refine discrimination among these units. Therefore, this information provides only a preliminary assessment of the stratigraphic age of SRs.

The large majority (97%) of the SRs in this study are found in units dated to the Amazonian epoch (Table 4). Slightly over half of them (55%) are in the middle and lower members of the Medusae Fossae Formation (units Amm and Aml, respectively), which are dated to the middle Amazonian. About one-third are in the knobby plains material south of Cerberus Palus (unit Apk), dated as lower Amazonian. The remainder are scattered approximately evenly, a few percent each, among the smooth plains unit in Cerberus Palus (Aps), the ejecta of craters on the MFF (Ac), and middle and upper Noachian units (Npl1 and Npl2, respectively). All the isolated, rounded SRs are located within Amazonian units (Table 1). Otherwise, no correlation of SR class and geological age is observed.

These preliminary stratigraphic data indicate that the large majority of visible SRs were formed during the emplacement of the lower and middle members of the Medusae Fossae Formation, which are dated as having been laid down during the early to middle Amazonian epoch (~3.0 Ga; Hartmann and Neukum, 2001). However, the relatively young age of these units may reflect erosion and not emplacement (see Section 5.2 below). A very small percentage of SRs on the Aeolis Mensae southern highlands are located on units dated to the Noachian (⩾3.5 Ga; Hartmann and Neukum, 2001). However, these SRs could have formed after the Noachian, for example, in a younger, thin mantling unit that has since eroded. Such an occurrence was demonstrated in the formation of the SRs (Fig. 8a) discussed in Section 3.3.3 above. Thus, in spite of a few SRs situated on Noachian-aged units, all SR formation may have been confined to that later period during which the lower and middle units of the western MFF were emplaced. We find this explanation simpler than hypothesizing that SR formation extended from the Noachian through the Amazonian.

4.2. Topographic context

The SRs are largely confined to elevations between approximately −1700 m and −2500 m (Table 1). This elevation range reflects the preferential location of most of the SRs around the edges of the western MFF lobes, especially in the topographic depression between the lobes (Fig. 9). A small number of SRs are located at lower elevations (approximately −2650 to −2750 m) on Cerberus Palus units (Aps and Apk) to the west and northeast of the lobes. About 5% of the SRs are located at higher elevations on top of the MFF lobes. The few SRs on the Noachian units have both the lowest elevations, where located within fretted terrain troughs, and the highest elevations, where located on the Aeolis Planum highlands (Fig. 9).

The preferential location of the SRs around the edges of the western MFF lobes is likely a result of exposure due to erosion at the MFF margins. Of the ~5% of SRs located on top of the MFF lobes, some are located at erosive plateaus within the MFF (Area04, Area07, and Area20) and the remainder is located at an impact crater (Area06). The clustering of SRs at the MFF margins, along

with some SRs at sites of MFF erosion, suggests that additional SRs remain unexposed within the volume of the western MFF lobes.

5. Discussion

5.1. Global context

This study has documented ~150 SRs in the Aeolis/Zephyria Plana based on THEMIS visible wavelength coverage through July 2007; future work may show some of these to be/have been connected or to reveal additional examples. These ~150 examples are found in an area of ~200,000 km². For comparison, approximately the same number of similar landforms has been recorded outside of the Aeolis and Zephyria Plana region in a preliminary global database of SRs on Mars (Williams, 2007). Thus, the SRs within this study region represent the greatest regional population and cover the largest contiguous area of SRs yet identified on Mars.

Globally, SRs on Mars are found on terrains that span the entire history of Mars from the Noachian to the Amazonian epoch (Williams, 2007, and references therein). Collectively, the Aeolis/Zephyria SRs are the youngest population of SRs, with 97% of them in Amazonian units. Their location largely within the Medusae Fossae formation is one of ~10% of SR locations in the global survey situated in the Martian lowlands. The SRs at this site show a range in individual morphology and network pattern rarely observed in a single region. Most SR locales exhibit a more uniform morphology (e.g., only thin SRs) and network configuration (e.g., only branched networks). The Aeolis/Zephyria Plana region is the only location known at present to exhibit SRs with wide (>200 m) flat tops and multi-layer configurations (e.g., Fig. 5).

Although limited in frequency, the occurrence of fans and/or deltas in association with feeder SRs documented in the Aeolis/Zephyria Plana has not been previously observed elsewhere on Mars and demonstrates the link between transport pathways and depositional sinks. Fan-shaped landforms on Mars are typically located within crater basins, although they have also been observed associated with other highland-lowland transitions such as near the mountainous southern rim of Isidis Planitia (Crumpler and Tanaka, 2003). Several dozen large-scale (10–40 km length) fans within late-Noachian and early Hesperian aged southern highland craters have been identified in THEMIS IR images (Moore and Howard, 2005; Pondrelli et al., 2005). In these settings, radial ridges have been interpreted to be the eroded remnants of distributary channel networks (e.g., Moore and Howard, 2005). Elevated valley-terminal deposits have been recognized within ~20 equatorial highland impact craters (Irwin et al., 2005, and references therein; Fassett and Head, 2005), and sub-kilometer fan-shaped landforms are located in Hesperian-aged Mojave crater (Williams et al., 2004a, 2004b; Williams and Malin, 2008). However, the Aeolis/Zephyria Plana lack impact craters and therefore it is not surprising that only one fan-shaped form is located within a crater (Fig. 8b). In contrast, five fan-shaped forms within the study region are found on erosional scarps at the eastern edge of the western-most MFF lobe and another fan-shaped form is located within the fretted terrain at the highland-lowland boundary (e.g., Fig. 8a; see Fig. 9 for context).

5.2. Comparison with elsewhere in the MFF and implications for formation timing

This work has focused on SRs observed in the western portions of MFF, in part because the features are so well expressed in this local region. However, that ease of identification of SRs is not the sole, or even the primary, reason for this localized investigation. Considerable effort has been undertaken in the geologic mapping of portions of eastern MFF (Fig. 1) (e.g., Bradley et al., 2002; Zimbelman, 2006), but to date not a single SR has been identified east of ~180° E. The eastern portions of MFF have been interpreted as the youngest of the MFF deposits while the western portions are identified as the oldest deposits, based on relative stratigraphic relationships (Scott and Tanaka, 1982, 1986; Greeley and Guest, 1987). In addition, fluvial channels buried by eastern MFF materials and interpreted to predate MFF deposition (e.g., Bradley et al., 2002) may instead be confined to the very lowest stratigraphic units of the MFF deposits. Taken together, these interpretations suggest that the relative timing of the events that formed the SR features was confined to only the earliest portions of MFF emplacement.

Both geologic mapping with MOLA topography (Zimbelman, 2006) and MARSIS radar sounding data (Watters et al., 2007) suggest that the eastern MFF deposits could be up to 2.5 km thick near the Gordii Dorsum escarpment (near 5° N, 215° E) (Fig. 1). This thickness is in marked contrast to the western MFF, where the deposits are all relatively thin (several tens to hundreds of meters in thickness) (Sakimoto et al., 1999; Bradley et al., 2002; Hynek et al., 2003; Watters et al., 2007). Either the thicker deposits in the eastern MFF have not been eroded to sufficient depth to expose the early time interval represented by the SRs in the western MFF, or SRs were no longer being formed when the later (upper) members of the eastern MFF were deposited. Future mapping and radar sounding should be able to test the relative importance of these alternative options.

5.3. Implications for origin: regional orographic precipitation

Our hypothesis is that most of the flat and multilevel SRs are aqueous paleoflow features, either inverted fluvial channels or eskers. The large majority (95%) of these features, including all the inferred eskers, are found in MFF stratigraphic units dated as early to middle Amazonian in age. Located in the middle and lower MFF units, the SRs must have formed syngenetically with these early units. However, these units may be late Hesperian in age. It is possible that the young (Amazonian) age universally associated with MFF materials may not be an emplacement age of the deposits but may be an exposure age of the surface, reflecting the ease with which impact craters can be removed by the erosion of the apparently friable MFF materials. Schultz and Lutz (1988) present observations of pedestal craters in the MFF materials, which they suggest can provide a constraint on the earliest age of MFF as being late Hesperian, an age that is much earlier in Mars' history than would be inferred from the relatively few impact craters currently visible on MFF surfaces (e.g., Werner, 2006). Thus, the lower and middle MFF units, and the SRs located therein, may date from the late Hesperian (Schultz and Lutz, 1988) to the middle Amazonian (Tanaka, 1986; Werner, 2006).

If our hypothesis for the features' origins is correct, then conditions at Mars' equator were sufficiently temperate and humid during the time that the lower and middle MFF units were being emplaced to form fluvial and glaciofluvial features. Young glacial features have been inferred elsewhere at Mars' equator. Sub-parallel ridges roughly concentric to a Mangala Fossa at the origination of Mangala Valles have been inferred to be moraines, deposited at the terminus of glaciers (Head et al., 2004). The origin of the Mangala moraines was deduced to be local snow fall generated by release of water from the fissure. However, that model does not seem applicable for the origin of the SRs in the western MFF, as no fissure source for the water is apparent.

The extensive area covered by this population of SRs (Fig. 9) and the large percentage (68%) of branched and sub-parallel SR networks within this population (Table 2) are consistent with formation of the population as a whole by a distributed water source. A distributed water source in turn suggests an atmospheric pro-

cess, namely, precipitation. Precipitation runoff is inferred for the formation of the inverted fluvial features, which are the flat, multilevel, and most thin SRs. Fluvial features can be supplied by groundwater sapping, but the branched and sub-parallel network morphologies are counterindicative of sapping. Our analysis of two of the SR networks associated with impact craters indicates that those networks also formed through runoff, either before or after crater formation (see Section 3.3.3). Precipitation runoff in the form of meltwater is also implied in the formation of eskers, because terrestrial eskers normally form as a result of meltwater from wet-based glaciers. Other sources may also be possible, for example, jökulhaups from a supraglacial lake draining through an ice-walled channel in a cold-based glacier could conceivably form esker-like deposits. However, at this time, our analysis does not support this atypical interpretation.

During early MFF emplacement, the location of this extensive SR population may have been a site of a topographic rise from (paleo)Cerberus Palus up to the Aeolis Planum highland. MARSIS radar data reveal that the MFF was emplaced over a relatively planar surface with a distinct elevational increase up to the Aeolis Planum (Watters et al., 2007). In these radar data, the elevational difference between this lower planar surface and the Aeolis Planum highland is ∼2500 m (Watters et al., 2007). This sharp and significant topographic rise shown in the MARSIS radar data would have caused orographic lifting of southward moving air masses. Orographic lifting, or lifting due to topography, results when an air mass is forced to move up an obstacle, such as a mountain. As the air mass increases in altitude up the obstacle, it cools. This cooling reduces its capacity to hold water vapor, which forms clouds and (given sufficient water vapor and/or orographic lifting) precipitation. Orographic precipitation occurs at coastal mountain ranges on Earth, producing rain shadow deserts in their lee. Examples of terrestrial rain shadowed regions include: the desert in eastern Washington state, leeward of the Cascade Mountains; the eastern Patagonia region in Argentina and Chile, which is shadowed by the Andes to the west; and the South Island of New Zealand, where the windward side of the Southern Alps annually receives several meters of liquid water equivalent precipitation which creates glaciers, whereas the leeward side receives less than a meter. (In all these examples, the prevailing winds are westerly.) As illustrated by these examples, orographic precipitation can occur as rain or as snow. Either rainfall runoff or snow melt could produce fluvial channels that are subsequently inverted. Accumulation of snowfall, if compacted into glaciers, could produce eskers.

In summary, on the basis of their topographic context, broad areal distribution, and network morphology, we hypothesize formation of these SRs as aqueous flow features resulting from orographic precipitation at the paleo-scarp between Cerberus Palus and the Aeolis/Zephyria Plana. Additional analysis, including atmospheric modeling and mapping of other glacial features, is required to test these hypothesized causes of SR formation.

6. Summary and future work

On the basis of morphology and slope information, we hypothesize that most of the SRs in the Aeolis/Zephyria Plana region are formed by aqueous surficial flow. Specifically, flat SRs are hypothesized to be inverted meandering fluvial channels or floodplains, with the exception of one flat SR on Cerberus Palus (Fig. 5d), which may be more likely a perched lava channel. Multilevel SRs are hypothesized to be stacked inverted fluvial features, in which the lower level was a meandering floodplain and the upper level was a single channel bed. Rounded SRs are tentatively hypothesized to be eskers on the basis of their individual morphology, network pattern, and local maxima in ridge elevation. Thin SRs are hypothesized to be inverted channels, whereas thin SRs with medial ridges

are tentatively hypothesized to be eskers on the basis of their morphological similarity to sharp-ridged terrestrial eskers. However, the pronounced sinuosity of rounded eskers and the general lack of other obvious glaciogenic landforms require further investigation. No formation mechanism is presented here for wispy SRs. Several fan-shaped forms are noted in this region, either alone or in association with SRs, and on the basis of (topographic) context are inferred to be water-lain. In addition to morphological and slope information, this association supports our hypothesis that the SRs are aqueous flow features. Some of the SRs are spatially associated with impact craters, but the data do not support a genetic relationship between the SRs and the craters.

These aqueous flow features are significant for several reasons:

- Qualitatively, they are the most densely clustered population of SRs on Mars. Especially along the edges of the MFF lobes, SRs are frequently contiguous and/or stratigraphically superposed.
- These SRs exhibit a wide variety of morphologies. Even contiguous or superposed examples are frequently different in both individual ridge and ridge network morphology.
- They occur at the equator, in contrast with most other longterm aqueous flow features, which are found in the southern highlands.
- These SRs are located at a paleoscarp along the highlandlowland boundary. This location, in conjunction with their broad areal distribution and network morphologies, leads to the hypothesis that their formation was due to runoff from orographic precipitation in the form of rain or snow.
- They are among the youngest SRs on Mars, found among units dating from the late Hesperian to the middle Amazonian.

Thus, these SRs imply geomorphologically significant precipitation on Mars at the equator at some time between the late Hesperian and middle Amazonian.

Continued work on these features will entail regional mapping using THEMIS IR, HRSC, and CTX data, which may reveal additional SRs and/or show connections among them. Along with HiRISE images, these data will allow determination of flow directions, which will be combined with topographic data to further constrain formation scenarios. Using MOLA topographic data, discharges will be calculated with either fluvial flow or esker flow models. These discharge values will then be used to constrain the climate necessary for producing these young, pervasive flow features at Mars' equator.

Acknowledgments

References

Banerjee, I., McDonald, B.C., 1975. Nature of esker sedimentation. In: Jopling, A.V., McDonald, B.C. (Eds.), Glaciofluvial and Glaciolacustrine Sedimentation. In: Soc. Econ. Paleontol. Mineral. Spec. Pub., vol. 23. SEPM, pp. 304–320.

Barnhart, C.J., Niimmo, F., Travis, B.J., 2008. Geophysical controls on martian post-impact hydrothermal systems. Lunar Planet. Sci. XXXIX, 1–17. Abstract 2294 (CD-ROM).

Bradley, B.A., Sakimoto, S.E.H., Frey, H., Zimbelman, J.R., 2002. Medusae Fossae Formation: New perspectives from Mars Global Surveyor. J. Geophys. Res. 107 (E8), doi:10.1029/2001JE001537. 5058.

Brennand, T.A., 2000. Deglacial meltwater drainage and glaciodynamics: Inferences from Laurentide eskers, Canada. Geomorphology 32, 263–293.

Brennand, T.A., 1994. Macroforms, large bedforms and rhythmic sedimentary sequences in subglacial eskers, south-central Ontario: Implications for esker genesis and meltwater regime. Sediment. Geol. 91, 9–55.

Burr, D.M., Williams, R.M.E., Nussbaumer, J., Zimbelman, J.R., 2006. Multiple, distinct, (glacio?)fluvial paleochannels throughout the western Medusae Fossae Formation, Mars. Lunar Planet. Sci. XXXVII, 1367.

Butzer, K.W., Hansen, C.L., 1968. Desert and River in Nubia. Univ. of Wisconsin Press, Madison. 497 pp.

Crumpler, L.S., Tanaka, K.L., 2003. Geology and MER target site characteristics along the southern rim of Isidis Planitia, Mars. J. Geophys. Res. 108 (E12), doi:10.1029/2002JE002040. 8080.

Edgett, K.S., 2005. The sedimentary rocks of Sinus Meridiani: Five key observations from data acquired by the Mars Global Surveyor and Mars Odyssey orbiters. Mars J. 1, 5–58.

El-Baz, F., Breed, C.S., Grolier, M.J., McCauley, J.F., 1979. Eolian features in the western desert of Egypt and some applications to Mars. J. Geophys. Res. 84 (B14), 8205–8221.

Fassett, C.I., Head III, J.W., 2005. Fluvial sedimentary deposits on Mars: Ancient deltas in a crater lake in the Nili Fossae Region. Geophys. Res. Lett. 32, doi:10.1029/2005GL023456. L14201.

Fedo, C.M., Finkelstein, D.B., Moersch, J., 2007. Alternative interpretations for the Eberswalde Delta, Holden NE Crater, Mars. In: Geol. Soc. Am. Annual Meet., Denver, 28–31 Oct. 2007, Paper No. 209-16.

Fishbaugh, K.E., Head, J.W., 2001. Comparison of the north and south polar caps of Mars: New observations from MOLA data and discussion of some outstanding questions. Icarus 154 (1), 145–161.

Gaddis, L., Anderson, J., Becker, K., Becker, T., Cook, D., Edwards, K., Eliason, E., Hare, T., Kieffer, H., Lee, E.M., Mathews, J., Soderblom, L., Sucharski, T., Torson, J., McEwen, A., Robinson, M., 1997. An overview of the integrated software for imaging spectrometers (ISIS). Lunar Planet. Sci. XXVIII, 387.

Gravenor, C.P., Kupsch, W.O., 1959. Ice-disintegration features in western Canada. J. Geol. 67 (1), 48–64.

Greeley, R., Guest, J.E., 1987. Geologic map of the eastern equatorial region of Mars. U.S. Geol. Surv. Misc. Invest., Map I-1802-B, 1:15,000,000.

Greeley, R., Kuzmin, R.O., Haberle, R.M., 2001. Aeolian processes and their effects on understanding the chronology of Mars. Space Sci. Rev. 96 (1/4), 393–404.

Hartmann, W.K., Berman, D.C., 2000. Elysium Planitia lava flows: Crater count chronology and geological implications. J. Geophys. Res. 105 (E6), 15011–15025.

Hartmann, W.K., Neukum, G., 2001. Cratering chronology and evolution of Mars. In: Kallenbach, R., Geiss, J., Hartmann, W.K. (Eds.), Chronology and Evolution of Mars. In: Space Sci. Rev., vol. 96. Kluwer Academic, Dordrecht, pp. 165–194.

Head, J.W., Kreslavsky, M.A., 2001. Medusae Fossae Formation as volatile-rich sediments deposited during high obliquity: An hypothesis and tests. In: Conf. Geophys. Detection of Subsurface Water on Mars. Abstract 7053.

Head, J.W., Pratt, S., 2001. Extensive Hesperian-aged south polar ice sheet on Mars: Evidence for massive melting and retreat, and lateral flow and ponding of meltwater. J. Geophys. Res. 106 (E6), 12275–12300.

Head III, J.W., Marchant, D.R., Ghatan, G.J., 2004. Glacial deposits on the rim of a Hesperian–Amazonian outflow channel source trough: Mangala Valles. Mars. Geophys. Res. Lett. 31, doi:10.1029/2004GL020294. L10701.

Hebrand, M., Åmark, M., 1989. Esker formation and glacier dynamics in eastern Skåne and adjacent areas, southern Sweden. Boreas 18, 67–81.

Holm, D.A., 1960. Desert geomorphology in the Arabian peninsula. Science 132, 1369–1379.

Howard, A.D., 1967. Drainage analysis in geologic interpretation: A summation. Am. Asoc. Petrol. Geol. Bull. 51, 2246–2259.

Howard, A.D., 1981. Etched plains and braided ridges of the south polar region of Mars: Features produced by basal melting of ground ice? Rep. Planet. Geol. Program, NASA TM 84211, 286–288.

Howard, A.D., 1991. Modeling channel migration and floodplain sedimentation in meandering streams. In: Carling, P.A., Petts, G.E (Eds.), Lowland Floodplain Rivers: Geomorphological Perspectives. Wiley, Chichester, pp. 1–41.

Howard, A.D., 1996. Modeling channel evolution and floodplain morphology. In: Anderson, M.G., Walling, D.E., Bates, P.D. (Eds.), Floodplain Processes. Wiley, Chichester, pp. 15–62.

Hynek, B.M., Phillips, R.J., Arvidson, R.E., 2003. Explosive volcanism in the Tharsis region: Global evidence in the martian geologic record. J. Geophys. Res. 108 (E9), doi:10.1029/2003JE002062. 5111.

Irwin III, R.P., Howard, A.D., Craddock, R.A., Moore, J.M., 2005. An intense terminal epoch of widespread fluvial activity on early Mars. 2. Increased runoff and paleolake development. J. Geophys. Res. 110, doi:10.1029/2005JE002460. E12S15.

Irwin III, R.P., Watters, T.R., Howard, A.D., Zimbelman, J.R., 2004. Sedimentary resurfacing and fretted terrain development along the crustal dichotomy boundary, Aeolis Mensae, Mars. J. Geophys. Res. 109, doi:10.1029/2004JE002248. E09011.

Jerolmack, D.J., Mohrig, D., Zuber, M.T., Byrne, S., 2004. A minimum time for the formation of Holden Northeast fan, Mars. Geophys. Res. Lett. 31, doi:10.1029/2004GL021326. L21701.

Kargel, J.S., Strom, R.G., 1992. Ancient glaciation on Mars. Geology 20 (1), 3–7.

Kargel, J.S., Baker, V.R., Beget, J.E., Lockwood, J.F., Pewe, T.L., Shaw, J.S., Strom, R.G., 1995. Evidence of ancient continental glaciation in the martian northern plains. J. Geophys. Res. 100 (E3), 5351–5368.

Keszthelyi, L.P., McEwen, A.S., Thordarson, Th., 2000. Terrestrial analogs and thermal models for martian flood lavas. J. Geophys. Res. 105 (E6), 15027–15050.

Keszthelyi, L.P., Thordarson, Th., McEwen, A.S., Haack, H., Guilbaud, M.-N., Self, S., Rossi, M.J., 2004. Icelandic analogs to martian flood lavas. Geochem. Geophys. Geosyst. 5, doi:10.1029/2004GC000758. Q11014.

King, L.C., 1942. South African Scenery. Oliver and Boyd, Edinburgh.

Kite, E.S., 2004. Evidence for ancient equatorial ice sheets on Mars? In: AGU Fall Meet. Program with Abstracts, P13A-0980.

Knight, J., 2002. Bedform patterns, subglacial meltwater events, and Late Devensian ice sheet dynamics in north-central Ireland. Global Planet. Change 35, 237–253.

Knighton, D., 1998. Fluvial Forms and Processes. Arnold, co-published by John Wiley and Sons, New York.

Knudsen, Ó., 1995. Concertina eskers, Brúarjökull, Iceland: An indicator of surge-type glacier behaviour. Quat. Sci. Rev. 14, 487–493.

Kolb, E.J., Tanaka, K.L., 2001. Geologic history of the polar regions of Mars based on Mars Global Surveyor data. II. Amazonian period. Icarus 154 (1), 22–39.

Kraal, E.R., Postma, G., 2008. The challenge of explaining meander bends in the Eberswalde Delta. Lunar Planet Sci.. Abstract 1897 (CD-ROM).

Leopold, L.B., Wolman, M.G., Miller, J.P., 1992. Fluvial Processes in Geomorphology. Dover Publications, New York.

Maizels, J.K., 1983. Palaeovelocity and palaeodischarge determination for coarse gravel deposits. In: Gregory, K.J. (Ed.), Background to Palaeohydrology. Wiley, New York, pp. 101–139.

Maizels, J.K., 1987. Plio-Pleistocene raised channel systems of the western Sharqiya (Wahiba), Oman. In: Frostick, L., Reid, I. (Eds.), Desert Sediments: Ancient and Modem. Geol. Soc. Spec. Publ., vol. 35. Geological Society, London, pp. 31–50.

Maizels, J.K., 1990. Raised channel systems as indicators of palaeohydrologic change: A case study from Oman. Palaeogeogr. Palaeoclimatol. Palaeoecol. 76, 241–277.

Malin, M.C., Edgett, K.S., 2003. Evidence for persistent flow and aqueous sedimentation on early Mars. Science 302, 1931–1934.

Mangold, N., Quantin, C., Ansan, V., Delacourt, C., Allemand, P., 2004. Evidence for precipitation on Mars from dendritic valleys in the valles Marineris Area. Science 305, 78–81.

Mann, A.W., Horowitz, R.C., 1979. Groundwater calcrete deposits in Australia: Some observations from Western Australia. J. Geol. Soc. Aust. 26, 293–303.

Mandt, K.E., de Silva, S.L., Zimbelman, J.R., Crown, D.A., 2008. The origin of the Medusae Fossae Formation, Mars: Insights from a synoptic approach. J. Geophys. Res., in press.

Matile, G.L.D., Groom, H.D., 1987. Late Wisconsinan Stratigraphy and sand and gravel resources in the Rural Municipality of Lac du Bonnet and Local Government District of Alexander. Manitoba Energy and Mines; Mines Branch, Aggregate Report 85-2, 44 pp. + 4 maps.

McEwen, A.S., Preblich, B.S., Turtle, E.P., Artemieva, N.A., Golombek, M.P., Hurst, M., Kirk, R.L., Burr, D.M., Christensen, P.R., 2005. The rayed crater Zunil and interpretations of small impact craters on Mars. Icarus 176 (2), 351–381.

McMenamin, D.S., McGill, G.E., 2005. Processes involved in the formation of martian fan-shaped deposits. Lunar Planet. Sci. XXXVI. Abstract 1732.

Moore, J.M., Howard, A.D., 2005. Large alluvial fans on Mars. J. Geophys. Res. 110, doi:10.1029/2004JE002352. E04005.

Moore, J.M., Howard, A.D., Dietrich, W.E., Schenk, P.M., 2003. Martian layered fluvial deposits: Implications for Noachian climate scenarios. Geophys. Res. Lett. 24, doi:10.1029/2003GL019002.

Murray, J.B., Muller, J.-P., Neukum, G., Werner, S.C., van Gasselt, S., Hauber, E., Markiewicz, W.J., Head, J.W., Foing, B.H., Page, D., Mitchell, K.L., Portyankina, G., The HRSC Co-Investigator Team, 2005. Evidence from the Mars Express High Resolution Stereo Camera for a frozen sea close to Mars' equator. Nature 434 (7031), 352–356.

Niem, A.R., 1974. Wright's point, Harney County, Oregon: An example of inverted topography. Ore Bin 36 (3), 33–49.

Nussbaumer, J., 2005. Extent and further characteristics of Former Glaciated Terrain in Elysium Planitia, Mars. Lunar Planet Sci. XXXVI. Abstract No. 1949.

Nussbaumer, J., 2007. Possible sea sediments due to glaciofluvial activity in Elysium Planitia, Mars. In: 7th Int. Conf. Mars. Abstract No. 1353, p. 3176.

Nussbaumer, J., Jaumann, R., Hauber, E., 2003. Evidence for a surging ice-sheet in Elysium Planitia, Mars. In: Sixth Int. Conf. Mars. Abstract 3018.

Orr, E.L., Orr, W.N., 2000. Geology of Oregon, fifth ed. Kendall/Hunt Publishing Company, Dubuque, Iowa, pp. 118–119.

Pain, C.F., Ollier, C.D., 1995. Inversion of relief—A component of landscape evolution. Geomorphology 12, 151–165.

Plescia, J.B., 2003. Cerberus Fossae, Elysium, Mars: A source for lava and water. Icarus 164, 79–95.

Poland, M., Miklius, A., Orr, T., Sutton, J., Thornber, C., Wilson, C., 2008. New episodes of volcanism at Kilauea Volcano, Hawaii. Eos 89 (5), 37–38.

Pondrelli, M., Baliva, A., Di Lorenzo, S., Marinangeli, L., Rossi, A.P., 2005. Complex evolution of paleolacustrine systems on Mars: An example from the Holden crater. J. Geophys. Res. 110, doi:10.1029/2004JE002335. E04016.

Reeves, T., 1983. Pliocene channel calcrete and suspenparallel drainage in West Texas and New Mexico. In: Wilson, R.C.L. (Ed.), Residual Deposits: Surface Related Weathering Processes and Materials. In: Geol. Soc. Spec. Publ., vol. 11. Backwell, Oxford, pp. 178–183.

Rhodes, D.D., 1980. Exhumed topography—A case study of the Stanislaus Table Mountain, California. Rep. Planet. Geol. Program, 397–399.

Rhodes, D.D., 1981. Exhumed topography—A review of some principles. Rep. Planet. Geol. Program, 316–318.

Röthlisberger, H., 1972. Water pressure in intra- and subglacial channels. J. Glaciol. 11, 177–203.

Russell, H.A.J., Arnott, R.W.C., 2003. Hydraulic jump and hyperconcentrated flow deposits of a glacigenic subaqueous fan: Oak Ridges Moraine, southern Ontario, Canada. J. Sediment. Res 73 (6), 887–905.

Sakimoto, S.E.H., Frey, H.V., Garvin, J.B., Roark, J.H., 1999. Topography, roughness, layering, and slope properties of the Medusae Fossae Formation from Mars Orbiter Laser Altimeter (MOLA) and Mars Orbiter Camera (MOC) data. J. Geophys. Res. 104 (E10), 24141–24154.

Schultz, P.H., Lutz, A.B., 1988. Polar wandering on Mars. Icarus 73, 91–141.

Schultz, P.H., Lutz-Garihan, A.B., 1981. Equatorial paleo-poles on Mars. Lunar Planet. Sci. XII, 946–948.

Scott, D.H., Morris, E.C., West, M.N., 1978. Geologic map of the Aeolis Quandrangle of Mars. U.S. Geol. Surv. Misc. Invest., Map I-1111, scale 1:5,000,000.

Scott, D.H., Tanaka, K.L., 1982. Ignimbrites of Amazonis Planitia region of Mars. J. Geophys. Res. 87 (B2), 1179–1190.

Scott, D.H., Tanaka, K.L., 1986. Geologic map of the western equatorial region of Mars. U.S. Geol. Surv. Misc. Invest., Map I-1802-A, scale 1:15,000,000.

Shetsen, I., 1987. Quaternary geology of southern Alberta. Alberta Res. Council Map, 1:500,000, 1 sheet.

Shreve, R.L., 1985. Esker characteristics in terms of glacial physics, Katahdin esker system, Maine. Geol. Soc. Am. Bull. 96, 639–646.

Smith, D.E., Zuber, M.T., Frey, H.V., Garvin, J.B., Head, J.W., Muhleman, D.O., Pettengill, G.H., Phillips, R.J., Solomon, S.C., Zwally, H.J., Banerdt, W.B., Duxbury, T.C., 1998. Topography of the Northern Hemisphere of Mars from the Mars Orbiter Laser Altimeter. Science 279 (5357), 1686–1692.

Sun, T., Meakin, P., Jøssang, T., 2001. Meander migration and the lateral tilting of floodplains. Water Resour. Res. 37 (5), 1485–1502.

Tanaka, K.L., 1986. The stratigraphy of Mars. J. Geophys. Res. 91, 139–158.

Tanaka, K.L., Chapman, M.G., Scott, D.H., 1992. Geologic map of the Elysium region of Mars. U.S. Geological Survey Map I-2147I.

Ward, A.W., 1979. Yardangs on Mars: Evidence of recent wind erosion. J. Geophys. Res. 84 (B14), 814–816.

Watters, T.R., Campbell, B., Carter, L., Leuschen, C.J., Plaut, J.J., Picardi, G., Orosei, R., Safaeinili, A., Clifford, S.M., Farrell, W.M., Ivanov, A.B., Phillips, R.J., Stofan, E.R., 2007. Radar sounding of the Medusae Fossae Formatiion Mars: Equatorial ice or dry, low-density deposits? Science 318, 1125–1128.

Wells, G.L., Zimbelman, J.R., 1997. Extraterrestrial arid surface processes. In: Thomas, D.S.G. (Ed.), Arid Zone Geomorphology: Process, Form and Change in Drylands. second ed. Wiley, New York, pp. 659–690.

Werner, S.C., 2006. Major aspects of the chronostratigraphy and geologic evolutionary history of Mars. Ph.D. dissertation, Freie Univ. Berlin, 165 pp., available from www.diss.fu-berlin.de/2006/33/indexe.html.

Williams, R.M.E., 2007. Global spatial distribution of raised curvilinear features on Mars. Lunar Planet Sci. XXXVIII. Abstract 1821.

Williams, R.M.E., Edgett, K.S., 2005. Valleys in the Martian rock record. Lunar Planet. Sci. XXXVI, 1099.

Williams, R.M.E., Malin, M.C., 2008. Sub-kilometer fans in Mojave Crater. Icarus 198, 365–383.

Williams, R.M.E., Malin, M.C., Edgett, K.S., 2004a. Young fans in equatorial crater in Xanthe Terra, Mars. Proc. Lunar Sci. Conf. 35. Abstract 1415.

Williams, R.M.E., Malin, M.C. Edgett, K.S., 2004b. Valleys and channels in the martian rock record. In: Workshop on Martian Valley Networks, August 11–14, 2004.

Williams, R.M.E., Malin, M.C., Edgett, K.S., 2005. Remnants of the courses of fine-scale, precipitation-fed runoff streams preserved in the martian rock record. Lunar Planet. Sci. Conf. XXXVI. Abstract #1173.

Williams, R.M.E., Chidsey Jr., T.C., Eby, D.E., 2007. Exhumed paleochannels in central Utah—Analogs for raised curvilinear features on Mars. In: Willis, G.C., Hylland, M.D., Clark, D.L., Chidsey Jr., T.C. (Eds.), Central Utah—Diverse Geology of a Dynamic Landscape. Utah Geological Association Publication, vol. 36. Salt Lake City, Utah.

Wood, L.J., 2006. Quantitative geomorphology of the Mars Eberswalde delta. Geol. Soc. Am. Bull. 118 (5/6), 557–566.

Zimbelman, J.R., 2006. Geologic mapping of the Medusae Fossae Formation on Mars and the northern lowland plains of Venus. U.S. Geol. Surv. Open File report, 2006 Planetary Geologic Mappers meeting, zimbelman_medusae-edited_final.pdf.

Zuber, M.T., Smith, D.E., Solomon, S.C., Muhleman, D.O., Head, J.W., Garvin, J.B., Abshire, J.B., Bufton, J.L., 1992. The Mars Observer Laser Altimeter investigation. J. Geophys. Res. 97, 7781–7798.